2009

Optimization of channel geometry in a proton exchange membrane (PEM) fuel cell

Jephanya Kasukurthi
University of Nevada Las Vegas

OPTIMIZATION OF CHANNEL GEOMETRY IN A PROTON EXCHANGE MEMBRANE (PEM) FUEL CELL

by

Jephanya Kasukurthi

Bachelor of Technology in Mechanical Engineering
Acharya Nagarjuna University, India
2007

A thesis submitted in partial fulfillment
of the requirements for the

Master of Science Degree in Mechanical Engineering
Department of Mechanical Engineering
Howard R. Hughes College of Engineering

Graduate College
University of Nevada, Las Vegas
December 2009

UNIVERSITY OF NEVADA LAS VEGAS

THE GRADUATE COLLEGE

We recommend that the thesis prepared under our supervision by

Jephanya Keerthi Swaroop Kasukurthi

entitled

Optimization of Channel Geometry in a Proton Exchange Membrane (PEM) Fuel Cell

be accepted in partial fulfillment of the requirements for the degree of

Master of Science
Mechanical Engineering

Yitung Chen, Committee Chair

Robert Boehm, Committee Member

Jianhu Nie, Committee Member

Yahia Bagzhouz, Graduate Faculty Representative

Ronald Smith, Ph. D., Vice President for Research and Graduate Studies
and Dean of the Graduate College

December 2009

ABSTRACT

Optimization of Channel Geometry in a Proton Exchange Membrane (PEM) Fuel Cell

by

Jephanya Kasukurthi

Dr. Yitung Chen, Examination Committee Chair
Professor of Department of Mechanical Engineering
University of Nevada, Las Vegas

Bipolar plates are the important components of the PEM fuel cell. The flow distribution inside the bipolar plate should be uniform. Non-uniform flow distribution inside the bipolar leads to poor performance of the fuel cell and wastage of expensive catalyst. A single channel PEM fuel cell is taken and electrochemical analysis is carried out on it. The results are compared with the available published experimental data obtained by other research group, and they are found to be in good agreement. A baseline design of the bipolar plate is taken and numerical analysis is carried out. The results show that the flow distribution is non-uniform. The baseline design is changed to an improved design to obtain a uniform flow. The improved design yielded a uniform flow. A single channel is taken from the improved design of the bipolar plate and electrochemical analysis is carried out on it. The geometry of the fuel cell channel is changed from rectangular to square, semi-circle and triangular shapes and the performances of the fuel cell are observed. The performance of the rectangular channel is found out to be the best, and the performance of the triangular channel is poor compared to rectangular channel design. The operating temperature of the fuel cell is varied and the results show that increasing the fuel cell temperature from 323K to 353K increases the fuel cell performance by 7.83%. Increasing the reaction temperature increases the thermal energy

available in the system and all the molecules in the system move about and vibrate with increased intensity increasing the rate of the reaction. The operating pressure of the fuel cell is varied, and the performance of the fuel cell is observed. The performance of the fuel increases by 2.35% when the pressure is increased by 2 atm on the anode side and 4 atm on the cathode side. The performance of the fuel cell increases due to a better supply of reactants at higher pressures to active sites.

TABLE OF CONTENTS

LIST OF FIGURES

LIST OF TABLES

NOMENCLATURE

a	water activity
A_m, A_{ch}	membrane area and channel cross section area (m^2)
b	Tafel slope
c	molar concentration (g-mole/cm^3)
D_{ij}	binary diffusivity (cm^2/s)
E^0	standard potential under 25 ^oC, 1 atm
F	Faraday constant (96487 C/mol)
ΔG^0	standard free energy (kJ/mol)
ΔH	stored chemical energy (kJ/mol)
I , I_{ref}	current (A) and reference current (A/m^2)
j	current density (A/m^2)
j_{sol} , j_{mem}	solid phase and membrane phase current density (A/m^2)
j_{an}^{ref} , j_{cat}^{ref}	volumetric reference exchange current density (A/m^2)
K	absolute permeability (cm^2)
K_r	relative permeability
k^{eff}	effective heat conductivity (W/m-K)
M_{w,H_2}	molecular weight of hydrogen (g/mol)
M_{w,H_2O}	molecular weight of water (g/mol)
M_{w,O_2}	molecule weight of oxygen (g/mol)
N	molar flux vector (g-mol/cm^2-s)
n	unit vector

p_c	capillary pressure (Pa)
p_{H_2} , p_{O_2}	hydrogen and oxygen gas pressure (Pa)
R	gas constant (8.314 J/K-mol)
R_{tol}	fuel cell total electric resistance (ohm)
r_w	condensation rate (kg/s)
s	liquid water saturation
T	absolute temperature (K)
U_i	velocity vector (m/s)
V_{cell}	fuel cell operating voltage (V)
V_{oc}	fuel cell open circuit voltage or ideal voltage (V)
w	weight fraction
X , x_i	molar fraction and molar fraction of species i
α_a , α_c	anode and cathode transfer coefficient
ε	porosity
σ_{sol} , σ_{mem}	solid and membrane field conductivity (Siemens)
σ	surface tension (N/m^2)
ϕ_{sol} , ϕ_{mem}	solid phase and membrane field potential (V)
φ , φ_i	fuel cell efficiency and ideal fuel cell efficiency
γ	concentration dependence
η_{mas}	mass transport limit loss potential (V)
η_{ohm}	ohmic loss potential (V)

η_{pol}	activation loss potential (V)
ρ_i	density of component i (kg/m^3)
ς_a, ς_c	anode and cathode stoichiometric ratio
μ_i	viscosity of component i (kg/m-s)
μ_l	liquid water viscosity (kg/m-s)

ACKNOWLEDGEMENTS

I would like to express profound gratitude to my advisor, Dr. Yitung Chen, for his invaluable support, encouragement, supervision and useful suggestions throughout this research work. His moral support and continuous guidance enabled me to complete my work successfully. This thesis would not have been possible without the kind support, the trenchant critiques, the probing questions, and the remarkable patience of my thesis advisor. I cannot thank him enough. I am also highly thankful to Dr. Jianhu Nie for his valuable suggestions throughout this study.

I would like to thank Dr. Robert F Boehm and Dr. Yahia Baghzouz for their time to review the thesis and for participation as defense committee members.

I am as ever, especially indebted to my parents, Dr. Ratna Raju and Mrs. Ruth Vindhya Vasini Kasukurthi for their love and support throughout my life. I am also thankful to my friends who made my life happy away from home

CHAPTER 1

INTRODUCTION

1.1 Background

Due to increasing pollution and depletion of the natural fuel resources an alternative for the energy sources have to be found out, in this process of uncovering the alternative fuel source, hydrogen energy has been found out [1]. The device which uses hydrogen as the fuel called fuel cell has been discovered in this process. It is believed that hydrogen can be a future solution to world's energy needs. "Fuel cell" is a device that combines hydrogen and oxygen to form water and electricity [1]. The produced energy can be used for our day to day needs. Fuel cells have many advantages when compared with the conventional devices. A Fuel cell has very high efficiency, and it is not limited by Carnot cycle efficiency [2]. Fuel cells are quiet and pollution free.

The development of the fuel cell began long back. In 1838 C.F.Schonbein developed "Fuel Cell theory" [3]. He conducted experiments and published results of producing electrical current using hydrogen and chlorine or oxygen gas on the platinum electrode and called this effect as "Polarization effect". In 1839 William R. Grove discovered "gas voltaic battery" [3]. He found that electrical energy is needed for producing hydrogen and oxygen gases from water electrolysis process and proposed that electrical energy can be produced from the reverse process. In 1889 L.Mond and C. Langer proposed the terminology of fuel cell. In 1902 Reid proposed the "alkaline fuel cell" concept [3]. In 1923 A. Schmidt proposed the "porous gas diffusion electrode" concept. Many developments took place after that. In 1966 DuPont developed the "Nafion" polymer or proton exchange membrane (PEM) [4]. In 1970 U.S. Department of

Energy developed molten carbonate fuel cell. In 1981 Westinghouse developed a solid oxide fuel cell. In 2003, 17 countries formed an international partnership for hydrogen economy (IPHE) to promote hydrogen energy and fuel cell technology research [4].

1.2 Advantages and Disadvantages of a Fuel Cell

A fuel cell is a device which combines hydrogen and oxygen to form water by electrochemical reaction and in this process electricity is produced. The battery is the electrochemical device we are familiar with. The chemicals stored in a battery are converted into electricity and go dead after they are used. The fuel cell works until the fuel is supplied continuously. There are many advantages for fuel cell. Fuel cell combines many advantages of both engines and batteries [2]. Fuel cells are more efficient than combustion engines because they produce electricity directly from chemical energy. Fuel cells don’t have any moving parts, so they are silent and mechanically ideal. The fuel cells are clean because they don’t emit harmful emissions. Fuel cells operate with higher energy densities compared to batteries and can be quickly recharged by refueling. There are some disadvantages of using fuel cells. Fuel cells are very expensive. The power density of fuel is less when compared with combustion engines and batteries. The fuel for the fuel cell is hydrogen. Hydrogen is not abundantly available, and the storage of hydrogen is also not easy. The operation temperatures are not compatible. Fuel cells are susceptible to environment poisons.

1.3 Types of Fuel Cells

There are five major types of fuel cells, differentiated from one another by their electrolyte:

1. Phosphoric acid fuel cell (PAFC)
2. Proton exchange membrane or polymer electrolyte membrane fuel cell (PEMFC)
3. Alkaline fuel cell (AFC)
4. Molten carbonate fuel cell (MCFC)
5. Solid oxide fuel cell (SOFC)

In 1961, G. V. Elmore and H. A. Tanner revealed new promise in phosphoric acid electrolytes in their paper “Intermediate Temperature Fuel Cells”, the stepping stone for phosphoric acid fuel cells [4]. Phosphoric acid fuel cells (PAFC) use phosphoric acid as the electrolyte and platinum as the catalyst. These fuel cells operate at a temperature range of around 160-200^{0}C. The efficiency of these fuel cells is around 37-42% [4]. The advantage of these fuel cells is that they can tolerate a carbon monoxide concentration of about 1.5%. Another advantage is that concentrated phosphoric acid electrolyte can operate above the boiling point of water, a limitation on other acid electrolytes that require water for conductivity. The application of these fuel cells is that they can be used for a thermal–electrical cogeneration power plant.

Proton exchange membrane fuel cell (PEMFC) is also called the polymer electrolyte membrane fuel cell. These fuel cells use proton conducting polymer membrane as electrolyte. Proton exchange membrane fuel cells operate at very low temperatures around 80^{0}C. PEMFC uses hydrogen as fuel and air as the oxidant and produces water as the by-product. These fuel cells are very useful because they operate at

low temperatures and high power density. The efficiency of these fuel cells is around 43 – 58 % [4]. PEMFC uses platinum as the catalyst. These fuel cells can mainly be used for transportation and automotive applications, so these fuel cells play a vital role for reducing the pollution of atmosphere. Proton exchange membrane fuel cells operate at very moderate temperatures, so they have low carbon monoxide tolerance which is a problem of poisoning of the catalyst (i.e. platinum) of the fuel cell.

Alkaline fuel cells (AFC) were developed in mid 1960's by NASA for the Apollo and space shuttle programs [4]. Alkaline fuel cells use an electrolyte that is an aqueous (water-based) solution of potassium hydroxide (KOH) retained in a porous stabilized matrix. The concentration of KOH can be varied with the fuel cell operating temperature, which ranges from 65°C to 220°C [4]. The charge carrier for an AFC is the hydroxyl ion (OH^-) that migrates from the cathode to the anode where it reacts with hydrogen to produce water and electrons. These are the cheapest fuel cells to manufacture when compared with other types of fuel cells. The disadvantage of these fuel cells is that they are very sensitive to carbon dioxide that may be present in fuel or air. The carbon dioxide reacts with the electrolyte, poisons it rapidly, and severely decreases the performance of the fuel cell. Due to these reasons the alkaline fuel cells are confined to closed environments such as space and undersea vehicles. Pure hydrogen and oxygen should be used for running these fuel cells. Alkaline fuel cells are not considered for automobile applications because of their sensitivity to poisoning.

Molten carbonate fuel cells (MCFC) are in the class of high temperature fuel cells. These fuel cells operate around a temperature of around 650^0C [4]. These fuel cells use an electrolyte composed of a molten mixture of carbonate salts. When these salts are

heated around 650^0C they melt and become conductive to carbonate ions (CO_3^{2-}). These ions flow from cathode to the anode where they combine with hydrogen to give water, carbon dioxide and electrons. The advantage of this fuel cell is that internal reforming is possible due to its high operating temperature. These fuel cells need significant time to reach the high temperature and respond slowly to power demands so these are suitable for constant power applications.

The solid oxide fuel cell (SOFC) is currently the highest temperature fuel cell in development. SOFC operates in a temperature range of 600^0C – 1000^0C [4]. Different kinds of fuels can be used because of the operating temperature. To operate at such high temperature these fuel cells use solid ceramic material (solid oxide) as the electrolyte material which is conductive to oxygen ions (O^{2-}). The charge carrier in the SOFC is the oxygen ion (O^{2-}). The operating efficiency of this fuel cell is highest, about 60% [4]. The high temperature of these fuel cells enables them to tolerate impure fuels such as those obtained from the gasification of coal or gasses from industrial processes. The startup time for these fuel cells is the main drawback, these fuel cells require significant amount of time to reach the operating temperature and respond slowly to the changes in electricity demand. Therefore these fuel cells are considered to be a leading candidate for high-power applications such as industrial and large-scale central-electricity generating-stations. These fuel cells require expensive materials for construction due to their high operating temperatures.

1.4 Basic Fuel Cell Operation

The electricity produced by a fuel cell increases with increase in reaction area. To provide large reaction surfaces fuel cells are usually made as thin and planar structures. One side of the planar structure of fuel cell is supplied with fuel and other side of the fuel cell is supplied with oxidant. A thin layer called electrolyte separates the fuel and electrodes and ensures that the two individual half reactions occur in isolation from one another. The major steps involved in producing electricity in a fuel cell are [2]:

1. Reactant delivery
2. Electrochemical reaction
3. Ionic conduction through the electrolyte and electronic conduction through the external circuit
4. Product removal from the fuel cell

Reactant transport: A fuel cell produces electricity when it is continuously supplied with fuel and oxidant. This seems to be a simple task but it is a very complicated process. When the fuel cell is operated at high current the demand for the reactants is very high. The reactants should be supplied rapidly otherwise the fuel cell will starve. The delivery of reactants can be effectively done by using the flow channels. The flow structures significantly affect the performance of the fuel cell [2]. The flow structure plays a vital role in the fuel cell performance because mass transport of the reactants can be controlled by the flow structure.

Electrochemical reaction: Immediately after the delivery the reactants should undergo electrochemical reaction. The current generated by the fuel cell depends on how fast the electrochemical reactions take place [2]. The faster the electrochemical reactions the

more is the current produced. The current produced is more if the electrochemical reaction is fast. High current from the fuel cell is desirable so catalysts are used to increase the speed and efficiency of the electrochemical reactions. The fuel cell performance vitally depends on choosing the right catalyst and carefully designing the reaction zones.

Ionic and electronic conduction: The electrochemical reactions produce or consume ions and electrons. Ions produced at one electrode must be consumed at the other electrode. This is also same for electrons. To maintain charge balance the electrons and ions must be transported from the place they are produced to the place they are consumed. Electrons can be transported easily whereas the transportation of ions is a tough task because ions are much larger and massive than electrons.

Product Removal: The fuel cells produce electricity with some by products for example H_2-O_2 fuel cell generate water, hydrocarbon fuel cells generate carbon dioxide (CO_2). The byproducts formed from the electrochemical reactions should be removed from time to time otherwise they will build up and eventually strangle the fuel cell and prevents new fuel and oxidant from reacting. The product removal is not one of the major issues of fuel cell designing but in PEMFC when the water is not removed it causes flooding of the fuel cell.

1.5 PEMFC

PEM stands for polymer electrolyte membrane or proton exchange membrane. A polymer membrane is present in the fuel cell so it is called a polymer electrolyte membrane. The polymer membrane has unique capabilities. It is impermeable to gases but it conducts protons so it is called a proton exchange membrane. The membrane is coated with thin layers of catalyst on either side and sandwiched between two porous gas diffusion layers (GDL) and these are collectively called as membrane electrode assembly which is place between two bipolar plates which supply fuel and oxidant for electrochemical reaction. The electrodes are manufactured with carbon cloth or carbon fiber paper. The catalyst material is platinum supported on carbon [4]. Electrochemical reaction takes place at the surface of the catalyst at the interface between the electrolyte and the membrane. Hydrogen is fed to the fuel and it splits into protons and electrons. The protons travel through the membrane where as the electrons travel through the collectors and external circuit to produce electricity. The protons formed from the hydrogen combine with the oxygen ions and produce water. The hydrogen side is negative and it is called the anode, whereas the oxygen side of the fuel cell is positive and it is called cathode.

1.6 Performance of a Fuel Cell

The performance of a fuel cell can be clearly identified from the graph of its current-voltage characteristics. The graph is called current density-voltage (j-V) curve, and it shows the voltage output of the fuel cell for a given current input. This curve is also called the polarization curve which is shown in Fig 1.1. The x-axis shows current

density i.e. current has been normalized by fuel cell area. Current density is used because a larger fuel cell can produce more electricity than a smaller fuel cell so that j-V curves are normalized by fuel cell area to make results comparable.

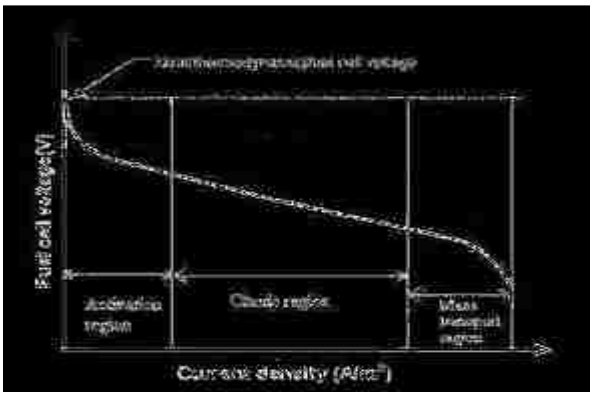

Fig 1.1 Polarization curve of a fuel cell

An ideal fuel cell continues to supply current until it is supplied with sufficient amount of fuel maintaining the constant thermodynamic voltage. The actual output of a real fuel cell is less than the ideal voltage or thermodynamic voltage. The voltage output of the fuel cell influences the total power produced. The power produced by the fuel cell is the product of current and voltage, P = iV. The power density curve gives the power density delivered by a fuel cell as a function of current density. The current supplied by a fuel cell is directly proportional to the amount of fuel consumed (i.e., if the fuel cell voltage decreases, the electric power produced by the fuel cell also decreases). By this relation we can say that fuel cell voltage is a measure of fuel cell efficiency. It is very important to maintain a constant voltage to have higher efficiency. It is very hard to maintain constant voltage due to the irreversible losses. The more the current drawn from

the fuel cell, the more are the losses. There are three major types of fuel cell losses which give the polarization curve the characteristic shape which can be seen in Fig.1.1. The three major losses are [2]:

a) Activation loss

b) Ohmic loss

c) Concentration loss

a) Activation loss:

The voltage which is sacrificed to overcome the activation barrier is called as the activation loss and it is represented as η_{act}. The Butler-Volmer equation is used to describe how current and voltage are related in electrochemical systems. The Butler-Volmer equation states that the current produced by an electrochemical reaction increases exponentially with activation overvoltage. This explains that if we want more current from the fuel cell we must pay a price in terms of lost voltage.

$$j = j_0^0\left(\frac{c_R^*}{c_R^{0*}} e^{\alpha nF\eta/(RT)} - \frac{c_P^*}{c_P^{0*}} e^{-(1-\alpha)nF\eta/(RT)}\right) \quad (1\text{-}1)$$

where η is the voltage loss, n is the number of electrons transferred in the electrochemical reaction, c_R^* and c_P^* are the actual surface concentrations of the rate-limiting species in the reaction, c_R^{0*} and c_P^{0*} are the product concentration values, j_0^0 represents the exchange current density at a standard concentration, F is Faraday constant and R and T are the gas constant and cell absolute temperature, α is the transfer coefficient. The empirical relationship between the activation overvoltage and the current density is given by the Tafel equation

$$\eta_{act} = a + b \log j \quad (1\text{-}2)$$

where a is the constant, b is the Tafel slope, and j is the current density.

b) Ohmic loss:

The voltage expended in order to accomplish charge transport is called the ohmic loss. It is represented as $\eta_{ohmic.}$

From Ohm's law

$$\eta_{ohmic} = iR_{ohmic} = i(R_{elec} + R_{ionic}) \quad (1\text{-}3)$$

where i is the current, and R_{elec} and R_{ionic} are the electronic and ionic resistances offered by the fuel cell. The electronic and ionic resistances depend on the material of the membrane.

c) Concentration loss:

The concentration loss is minimized by the careful optimization of mass transport in the fuel cell electrodes and fuel cell flow structures. It is represented as $\eta_{conc.}$

$$\eta_{conc} = c \ln \frac{j_L}{j_L - j} \quad (1\text{-}4)$$

where c is a constant which can be approximately given as

$$c = \frac{RT}{nF}\left(1 + \frac{1}{\alpha}\right) \quad (1\text{-}5)$$

j_L is the limiting current density which can be given as below

$$j_L = nFD^{eff}\frac{c_R^o}{\delta} \quad (1\text{-}6)$$

$$D_{ij}^{eff} = \varepsilon^{1.5} D_{ij} \quad (1\text{-}7)$$

where F is Faraday constant, D_{ij} is the binary diffusion coefficient (cm^2/s), ε is the porosity of the porous structure, D^{eff} is the effective diffusivity, c_R^o is the concentration of the reactants, n is the number of electrons transferred and δ is the gas diffusion layer thickness.

Fig.1.1 shows the polarization curve which has three regions activation, ohmic and mass transport region which are influenced by the losses in the fuel cell. The activation loss is predominant in the activation region of the polarization curve. The electrode kinetics controls the activation region. The loss at the ohmic region of the polarization curve is due to the ionic and electronic resistances provided by the fuel cell. The concentration loss is most significant at the tail of the polarization curve (i.e., in the mass transport region). This loss is due to the mass transport configuration of the fuel cell.

1.7 Literature Review

The physics involved in a fuel cell are very complicated. There are many processes simultaneously occurring in a PEM fuel cell. It is difficult to study every process that is involved in a fuel cell. Different researchers have concentrated on different aspects of fuel cell. The experimental setup for a fuel cell is very expensive so computational fluid dynamics (CFD) modeling has played a major role in the fuel cell research. The CFD model should be coupled with an electrochemical model to predict the species transport and electrochemical reactions.

Large numbers of numerical models of fuel cells have been developed by many researchers from the dawn of CFD. First the researchers have concentrated only on the

specific parts of the PEM fuel cell such as the bipolar plate, catalyst layer, gas diffusion layer and membrane. Some years back there was limited computational power so only a one- dimensional numerical model of PEM fuel was developed by Bernardi et al. [5] and the results were compared with experimental results. Later, two-dimensional numerical models were developed. The two-dimensional and one-dimensional models are only used to estimate the fuel cell performance but not very accurate. After the increase in computational power the three-dimensional models have been developed to analyze the fuel cell operation.

The three-dimensional models can approximately predict the behavior of the PEM fuel cell, but the processes involved in the fuel cell are very complicated so some assumptions have to be considered to simplify the modeling of the fuel cell. Dutta et al. [6] and Berning et al. [7] developed the three-dimensional models and have done research on them. Berning et al. [7] have performed parametric study for 3-D model of the PEM fuel cell and compared with experimental results obtained by Ticianelli et al. [8]. The experimental results obtained by Ticianelli et al. [8] have been used by many researchers to validate their numerical results. Djilali et al. [9], [10] discussed about the advanced computational tools for designing PEM fuel cell in two papers. Mann et al. [11] developed an electrochemical model of the PEM fuel cell and compared the results with a commercial Ballard PEM fuel cell. Nguyen et al. [12] developed a three-dimensional CFD model of a PEM fuel cell with serpentine flow field. They implemented a voltage-to-current (VTC) algorithm that solves for the potential as well as the local activation potential.

The PEM fuel cell consists of many parts such as bipolar plates, gas diffusion layers, catalyst layers and membrane. Every part plays an important role in the operation of the fuel cell. It is difficult to concentrate on every part so many researchers have concentrated on one of the parts or an aspect of the fuel cell. The bipolar plate has many functions such as supplying the fuel, draining out the byproduct water and collecting the current produced. The design of the flow structure that is present in the bipolar plate plays an important role in the performance of the fuel cell. There are many types of flow field designs: (1) parallel channel, (2) serpentine channel, (3) parallel serpentine channel, and (4) interdigitated channel. The fuel should be distributed uniformly otherwise there will be poor performance and inefficient use of the very expensive catalyst.

The serpentine flow field is mostly commonly used for a PEM fuel cell. Dutta et al. [13] developed a model to predict the mass flow between channels in a polymer electrolyte membrane (PEM) fuel cell with a serpentine flow path. Kazim et al. [14] developed a simple mathematical model to investigate the superiority of the interdigitated flow field design over the parallel flow field. The results obtained from their study show that the interdigitated flow field can double the maximum power density of a PEM fuel cell when compared with the parallel flow field. The modeling results agreed well with the experimental studies in their study. Park et al. [15] conducted numerical and experimental study to investigate the cross flow in a PEM fuel cell.

Grigoriev et al. [16] dealt with numerical optimization of the dimensions of channels and current transfer ribs of bipolar plates. The material of the bipolar plate also plays an important role in the performance of the fuel cell. Wind et al. [17] have done the research on using stainless steel as the material for the bipolar plate. Stainless steel with

thin coatings is suggested for the PEM fuel cell because the performance of the fuel cell with graphite bipolar plates is same as that of the fuel cell with coated metallic bipolar plates. Two types of carbon composite materials are developed by Cho et al. [18].

The membrane is the main component in PEM fuel cell. The fuel cell is named from the membrane's properties as proton exchange membrane or polymer electrolyte membrane. The membrane must exhibit properties such as high proton conductivity and low ionic conductivity, it should also act as a barrier to mixing of fuel and reactant gases, and it must be chemically and mechanically stable in the fuel cell environment. The membranes for PEM fuel cells are made of perflurocarbon-sulfonic acid ionomer (PSA). The best known membrane material is Nafion® made by Dupont. The protonic conductivity of a polymer membrane is strongly dependent on its membrane structure and its water content. The protons from one side of the membrane are dragged to the other side of the membrane with the help of water (called electroosmotic drag). Sgrecciaa et al. [19] developed self-assembled nano composite organic–inorganic proton conducting sulfonated poly-ether-ether-ketone (SPEEK)-based membranes for PEM fuel cells. Different strategies have been explored by them to improve water retention and morphological stability of sulfonated aromatic polymers. Mechanical and thermal properties, water uptake, and proton conductivity of the new membrane material are reported.

Yan et al. [20] conducted water balance experiments on the membrane of the fuel cell and found out that the net drag coefficient of water through the membrane depended on current density and humidification of feed gases. The diffusion of water across Nafion membranes was also investigated by experimental water flux measurements. PEM

membrane requirements are discussed in terms of two different parameters: temperature and relative humidity by Beuscher et al. [21]. Additional advancements will be necessary to meet aggressive operating conditions of higher temperatures and/or lower humidities, as well as longer operating lifetimes. In this paper, these challenges for fuel cell membranes are considered. The effect of operating parameters on the proton conductivity of PEM fuel cell membranes and the resulting effect on fuel cell performance are examined using experimental observations. Numerical simulations are used to assess the influence of water transport properties on the local hydration state of the membrane inside the running fuel cell.

The gas diffusion layer (GDL) is one of the critical components acting both as the functional as well as the support structure for membrane–electrode assembly in the proton exchange membrane fuel cell (PEMFC). Cindrella et al. [22] have studied the importance of the GDL of the PEMFC, reviewed the essential properties of the GDLs, and considered the methods of achieving each one of them. The paper also discusses the key parameters of the GDL such as structure, porosity, hydrophobicity, hydrophilicity, gas permeability, transport properties, water management and the surface morphology. They conducted extensive research and found out that it is very important to develop highly functionalized GDL with self–adjusting characteristics of water retention and water draining along with structural features to steadily supply the reactant gases to the catalyst.

Niu et al. [23] developed a multiphase, multiple-relaxation-time lattice Boltzmann model to study water-gas transport processes in the gas diffusion layer of a PEM fuel cell. The model is based on the diffuse interface theory, and employs two distributions so that

multiphase flows with large density ratios and various viscosities can be handled. In this paper water-gas transportation in a three-dimensional modeled GDL structure is simulated and the transport properties including absolute and relative permeabilities are calculated. Benziger et al. [24] studied how the water flows in a GDL of a PEM fuel cell. They conducted experiments and measured how the water flows through the GDL. They also found out how much pressure is required for the water transport through the GDL. They studied the pores that are present in the GDL and found the optimum pressure that is required to drain the water through the largest pores.

One of the most important parts of the PEM fuel cell is the catalyst layer. The electrochemical reactions take place on the surface of the catalyst. This is because three kinds of species participate in the electrochemical reactions namely gases, electrons and protons. Therefore the reactions take place on a portion of the catalyst where all the three species have access. The material used for the catalyst layer of PEM fuel cells is platinum. Zhang et al. [25] in their paper discuss the impact of degradation of the catalyst. This paper reviews the recent research on degradation and durability issues in the catalyst layers. They also suggested many experimental methods and investigation techniques for evaluating catalyst degradation.

Zhang et al. [26] performed quantitative analysis of catalyst layer degradation with X-ray photoelectron spectroscopy (XPS). XPS is quantitative, surface-sensitive, and able to distinguish different bonding environments or chemical states of fuel cell catalyst layers. The above capabilities are used to explore the complex mechanisms of degradation during fuel cell operation. Das et al. [27] developed a three–dimensional agglomerate model for cathode catalyst layer of PEM fuel cell. A finite element

technique is used for the numerical simulation is developed. Three configurations of agglomerate arrangements are simulated to investigate the oxygen transport process through the cathode catalyst layer and its impact on the activation polarization.

Hartnig et al. [28] worked on investigation of water drop kinetics and optimization of channel geometry for PEM fuel cell cathodes. The paper discussed about employing different flow field channel geometries and compared by means of a simplified parametric identification. The rectangular shaped channel with a width of 1 mm and a depth of 0.5 mm is found to exhibit best water removal properties at a reasonable pressure drop. Kuo et al. [29] performed numerical simulations to evaluate the convective heat transfer performance and velocity flow characteristics of gas flow channel design to enhance the performance of PEM fuel cell. The flow channel geometry is not changed but induced different types of interruptions for the gas channel. They implemented different types of obstacles such as wave like, trapezoid like and ladder like forms and straight channel. The numerical results obtained show that the channels with interruptions like wave, trapezoid and ladder like geometries increase the gas flow velocity in the channel and improve the catalysis reaction performance in the catalyst layer.

Wang et al. [30] developed a three-dimensional numerical model to explore the effects of the cathode flow channel configuration. They have found that the interdigitated design has superior cell performance over the parallel design for all the conditions considered. Their study considered the effects of the flow channel aspect ratio and flow channel cross-sectional area. They also found that the optimal flow channel aspect ratio is 1 and optimal cross-sectional area is 1mm x 1mm for the best cell performance.

1.8 Research Objectives

- Create a single channel PEMFC numerical model with the nine zones of two bipolar plates, two gas channels, two gas diffusion layers, two catalyst layers and a membrane.
- Simulate the hydrodynamic, heat transfer and electrochemical phenomena and obtain the fuel cell performance and validate the model using available published experimental data.
- Design bipolar plates with uniform flow distribution and take a single channel and carry out analysis on the single channel.
- Change the channel geometry of the fuel cell and compare the performance.

1.9 Thesis Outline

In this thesis, the channel geometry in a PEMFC is optimized and the performance studied. Chapter 2 explains the PEMFC modeling and the fundamentals of the electrochemistry involved in a fuel cell. The developed model is validated using a three-dimensional single channel PEMFC case. Chapter 3 discusses about designing a uniform flow bipolar plate for a PEMFC. Chapter 4 focuses on optimizing the channel geometry in a PEMFC. Chapter 5 concludes the current research and provides some future recommendations.

CHAPTER 2

PEM FUEL CELL NUMERICAL MODEL VALIDATION

2.1 Numerical Model of PEM Fuel Cell

A schematic view of the system considered is shown in Fig.2.1. A PEM fuel cell consists of nine zones. They are two gas channels, two bipolar plates, two gas diffusion layers, two catalyst layers and a membrane. The membrane is placed between two catalyst layers and then these are sandwiched between the gas diffusion layers and this assembly is placed between two bipolar plates. The bipolar plates consist of flow channels which provide fuel and oxidant for electrochemical reaction to take place. The fuel and oxidant diffuse from their respective sides through the gas diffusion layers and reactions take place at the catalyst layers and break down into ions and electrons. The electrons are collected and passed through an external circuit to produce electricity. The hydrogen ions formed from the electrochemical reaction combine with oxygen ions formed from the electrochemical reaction on the other side to form water. The chemical reactions that take place in the fuel cell are:

At anode: $2H_2\,(g) \longleftrightarrow 4H^+ + 4e^-$ (2-1)

At cathode: $4H^+ + 4e^- + O_2\,(g) \longleftrightarrow 2H_2O\,(l)$ (2-2)

Overall: $2H_2\,(g) + O_2\,(g) \longleftrightarrow 2H_2O\,(l)$ (2-3)

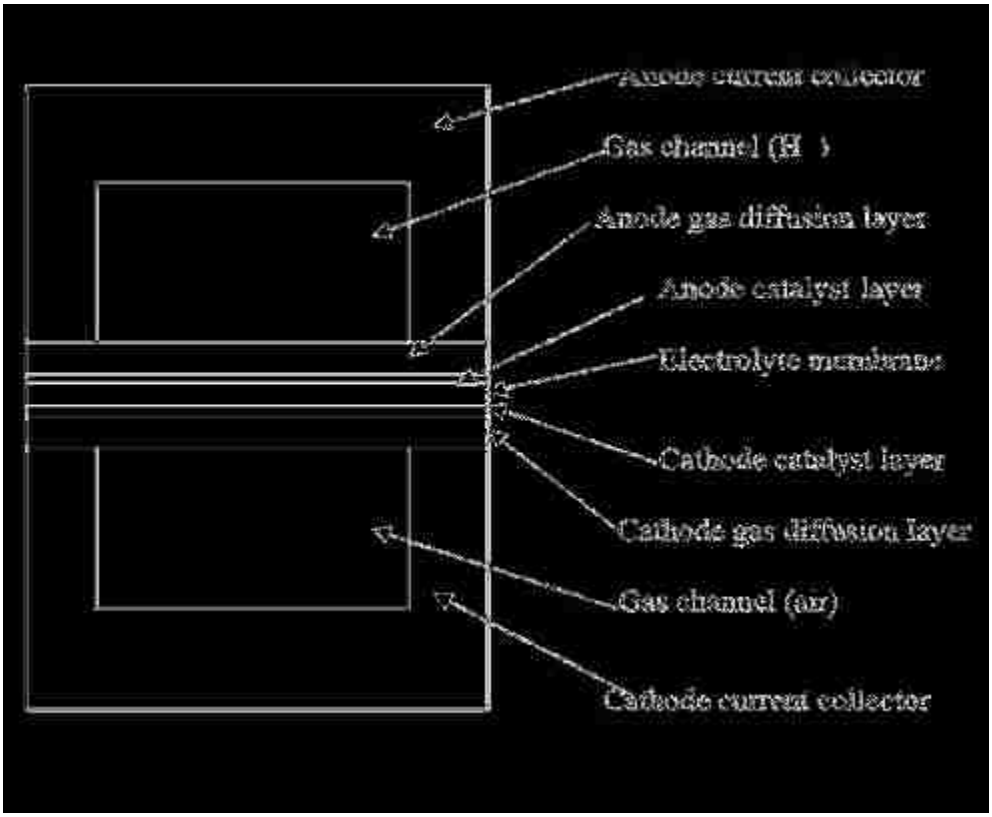

Fig 2.1 Schematic view of a typical PEMFC

The physics involved in a fuel are very complicated. To replicate a model of a fuel cell it is required to understand the mass, momentum and energy transport, electrochemical reactions and charge balance inside the fuel cell. To simplify the numerical modeling some assumptions are considered. They are:

- Ideal gas mixtures
- Steady state operation
- Isotropic electrodes and membrane
- Negligible contact resistance of current collector and MEA
- Incompressible flow

2.1.1 PEMFC Electrochemical Reactions

The electrochemical reactions involve both a transfer of electrical charge and a change in Gibbs energy. The rate of an electrochemical reaction is determined by an activation barrier. The speed at which an electrochemical reaction proceeds is the rate at which the electrons are released, which is the electrical current. Current density is the current per unit area of the surface. According to Faraday's law current density is proportional to the charge transferred and consumption of reactant per unit area [2].

$$i = nFv \tag{2-4}$$

where $(dN/dt = v)$ is the rate of the electrochemical reaction (mol/s), F is the Faraday's constant, n is the number of moles of electrons transferred during the electrochemical reaction.

2.1.2 Charge Balances

The electronic charge balance in the anode and cathode current collectors is given by

$$\nabla \bullet \left(-\sigma_1 \nabla \phi_{elec}\right) = 0 \tag{2-5}$$

where σ_1 denotes the electronic conductivity of the current feeder and ϕ_{elec} is its electronic potential.

The charge balance for the membrane is given by

$$\nabla \bullet \left(-\sigma_2 \nabla \phi_{ionic}\right) = 0 \tag{2-6}$$

where σ_2 is the ionic conductivity and ϕ_{ionic} is the potential in the membrane.

The electrochemical reactions take place on the surface of the catalyst and the protons are transferred through the membrane and the electrons are transferred back to the anode current collector. The electrons reach the cathode current collector through an external circuit. The charge balance is given by [31].

$$\nabla \bullet \left(-\sigma_1 \nabla \phi_{elec}\right) = S_a i_{ict} \tag{2-7}$$

$$\nabla \bullet \left(-\sigma_2 \nabla \phi_{ion}\right) = S_a i_{ict} \tag{2-8}$$

where $S_a i_{ict}$ denotes the specific surface area S_a times the charge transfer current reaction density i_{ict}.

To solve the equations the boundary conditions are specified as:

$$\phi_{elec} = 0 \quad \text{(anode)} \tag{2-9}$$

$$\phi_{elec} = V_{cell} \quad \text{(cathode)} \tag{2-10}$$

Butler-Volmer charge transfer kinetics describe the charge transfer current density. At the anode, hydrogen is reduced to form water, and the following charge transfer kinetics equation thus applies [31]:

$$i_{a.ct} = i_{0,a} x_{H_2} \frac{c_t}{c_{H_2.ref}} \left[\exp\left(\frac{\alpha F \eta}{RT}\right) - \exp\left(\frac{-(1-\alpha) F \eta}{RT}\right) \right] \tag{2-11}$$

where $i_{a.ct}$ is the current density at the anode, $i_{0,a}$ is the anode exchange current density (A/m^2), x_{H_2} is the molar fraction of hydrogen, c_t the total concentration of the species (mol/m^3), and $c_{H_2,ref}$ is the reference concentration (mol/m^3). Furthermore, F is the Faraday's constant (96500 C/mol), R the gas constant (J/ (mol-K)), T is the temperature (K) and η is the overvoltage (V).

For the cathode, the following applies [31]:

$$i_{c.ct} = i_{0,c} x_{O_2} \frac{c_t}{c_{O_2.ref}} \left[\exp\left(\frac{\alpha F \eta}{RT} \right) - \exp\left(\frac{-(1-\alpha) F \eta}{RT} \right) \right] \tag{2-12}$$

where $i_{c.ct}$ is the current density at the cathode side, $i_{0,c}$ is the cathode exchange current density (A/m^2), and x_{O_2} is the molar fraction of oxygen.

During the chemical reaction, the driving force is the overpotential between the solid electronic phase ϕ_{elec} and the ionic phase ϕ_{ion}, which is also known as the activation loss η. The overpotential is defined as:

$$\eta = \phi_{elec} - \phi_{ion} - \Delta\phi_{eq} \tag{2-13}$$

where $\Delta\phi_{eq}$ is the equilibrium potential difference (V).

At the cathode side, the cell voltage V_{cell} is defined as:

$$V_{cell} = \Delta\phi_{eq,c} - \Delta\phi_{eq,a} - V_{pol} \tag{2-14}$$

where V_{pol} is the polarization voltage. In this study, $\Delta\phi_{eq,a}$ = 0 V and $\Delta\phi_{eq,c}$ = 1 V and V_{pol} are treated as the parameters. For ionic charge balance equations, applying adiabatic boundary conditions at all external boundaries and for the interior boundaries, continuity in current and potential apply by default.

2.1.3 Mass Conservation Equations

In the present numerical model the mass conservation equation has different source terms in different cell zones. Generally, the mass conservation equation is expressed as:

$$\nabla \bullet \left(\rho_i U_i\right) = S_{mass} \tag{2-15}$$

where ρ_i is the density of species i, U_i is the velocity vector of species i, and S_{mass} is the source term. In the gas channel, as well as the gas diffusion layers and membrane, the source term S_{mass} is set to zero. In the catalyst layer, there are hydrogen/oxygen consumption and water formation. The mass sink and source rates depend on the electrochemical reaction rates. Thus, they can be calculated by:

$$S_{H_2} = -\frac{M_{w,H_2}}{2F} i_{an} \tag{2-16}$$

$$S_{O_2} = -\frac{M_{w,O_2}}{4F} i_{cat} \tag{2-17}$$

$$S_{H_2O} = \frac{M_{w,H_2O}}{2F} i_{cat} \tag{2-18}$$

where M_w is the molecular weight.

2.1.4 Momentum Conservation Equations

In the porous media regions, such as the gas diffusion layer and membrane, the momentum equation has to be modified as:

$$\frac{1}{\varepsilon(1-s)} \nabla \cdot \left(\rho_i U_i U_i\right) = -\nabla p_i + \frac{1}{\varepsilon(1-s)} \nabla \cdot \left(\mu_i \nabla U_i\right) + S_m \tag{2-19}$$

where s is the liquid water saturation, ε is the porosity, μ_i is gas viscosity (kg/m-s), p_i the pressure (Pa) . The source term S_m is set to be zero at the gas channel and membrane zones. In the diffusion layer and the catalyst layer, it is calculated based on the absolute permeability K and relative permeability K_r [32]:

$$S_m = -\frac{\mu_i}{K \cdot K_r} U_i \tag{2-20}$$

For the liquid, K_r is:

$$K_r = s^3 \tag{2-21}$$

For the gas phase, K_r is:

$$K_r = (1-s)^3 \tag{2-22}$$

2.1.5 Species Conservation Equation

For the PEMFC, in order to model the multi-species transport, the Maxwell-Stefan equation is a proper one to analyze those kinds of phenomena [33]:

$$\nabla x_i = -\sum_{j=1}^{N} \frac{1}{cD_{ij}} \left(x_j N_i - x_i N_j \right) \tag{2-23}$$

where c is the molar concentration (g-mole/cm^3), N is the molar flux vector (g-mole/cm^2-s), x_i and x_j are the mole fractions of components i and j . To determine the binary diffusivity D_{ij} (cm^2/s), the reference diffusivity has been used [34]:

$$D_{ij} = \varepsilon^{1.5} (1-s)^{2.5} D_{ij}^0 \left(\frac{p_0}{p} \right) \left(\frac{T}{T_0} \right)^{1.5} \tag{2-24}$$

Here the reference diffusivity D_{ij}^0 is the property based on reference pressure p_0, 101325 Pa, and reference temperature T_0, 300 K.

Fluid flow in porous media is model by Darcy's law since the gas diffusion layer and catalyst layer are assumed to be the homogeneous porous media.

$$U_i = -\frac{K_p}{\mu_i}\nabla p_i \tag{2-25}$$

where K_p is permeability (m^2) and μ_i is gas viscosity (kg /m-s).

The species balance in the porous gas diffusion electrode can be solved by the following equation:

$$\nabla \bullet \left(-\rho w_i \sum \left(D_{ij}\nabla x_j + \left(x_j - w_j\right)\frac{\nabla p}{p} \right) + \rho w_i U \right) = 0 \tag{2-26}$$

where w is the weight fraction, ρ is the mixture density (kg/m^3), which can be calculated by:

$$\rho = \frac{\sum_i x_i M_{w,i}}{RT} p \tag{2-27}$$

where $M_{w,i}$ is the molecular weight, R is the gas constant, T is the absolute temperature (K), x_i is the mole fraction of component i, p is the pressure (Pa) .

2.1.6 Energy Conservation

During the electrochemical reaction, the heat source includes the ohmic heat and reaction heat. In different zones, the heat source is different, such as in cathode catalyst, the reaction heat is the primary part; while in membrane, ohmic heat is the main heat source. The energy equation can be written as:

$$\nabla \cdot \left(\rho_i U_i T\right) = \nabla \cdot \left(k^{eff}\nabla T\right) + S_T \tag{2-28}$$

where $S_T = I^2 R_{ohm} + h_{reaction} + \eta_{an} i_{an} + \eta_{cat} i_{cat}$, k^{eff} is the effective heat conductivity (W/m-K), I is the electric current (A), R is the electric resistance (ohm), $h_{reaction}$ is the enthalpy (kJ/kg-K).

2.2 Numerical Model

The finite element method has been applied to simulate the transport phenomena in the present model of PEMFC. In the finite element method, the computational domain is discretized into a number of continuous finite elements. The partial differential governing equations are integrated over each control volume into a set of discretized equations. In the current simulations, the commercial software COMSOL® is used to generate the computational mesh and also the simulations are done using this software. For the heat transfer simulations the commercial software GAMBIT® is used to generate the computational mesh and then loaded into the CFD software Fluent® for the analysis.

2.2.1 Computational Domain

To validate the present numerical model, a single channel of the PEMFC is considered. The three-dimensional model of the single channel of the PEMFC consists of nine zones which are anode current collector, cathode current collector, anode gas channel, cathode gas channel, anode gas diffusion layer, cathode gas diffusion layer, anode catalyst layer, cathode catalyst layer and membrane. The dimensions of the numerical model are listed in Table 2.1 and are shown in Figure 2.2. The dimensions are taken from the work published by Ticianelli et al. [8].

Table 2.1 Dimensions of single channel PEMFC model

Dimension	*Value*
Gas channel length	40 mm
Gas channel width	1.0 mm
Gas channel height	0.8 mm
Diffusion layer height	0.26 mm
Catalyst layer height	0.01 mm
Membrane height	0.23 mm
Current collector width	1.8 mm
Current collector height	1.0 mm

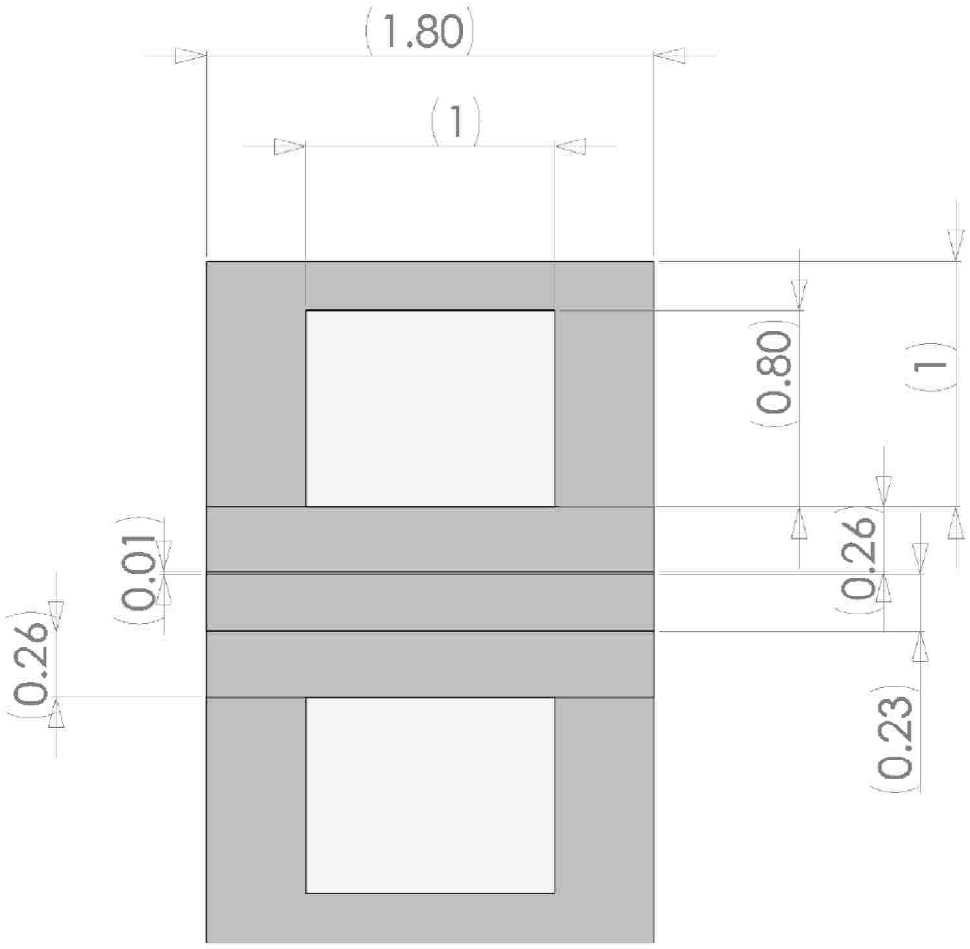

Fig 2.2 Dimensions of single channel PEMFC (Unit: mm)

From the above Fig 2.2, we can observe the dimensions of the single channel of PEMFC. The catalyst layer is very thin and has a thickness of about 10 micron. The membrane with the catalyst layers and gas diffusion layer collectively called as the membrane electrode assembly. The catalyst layer is sandwiched between the membrane and the GDL. In the actual fuel cell there will be a large number of channels, but for the purpose of validation of the model one of the channels is considered.

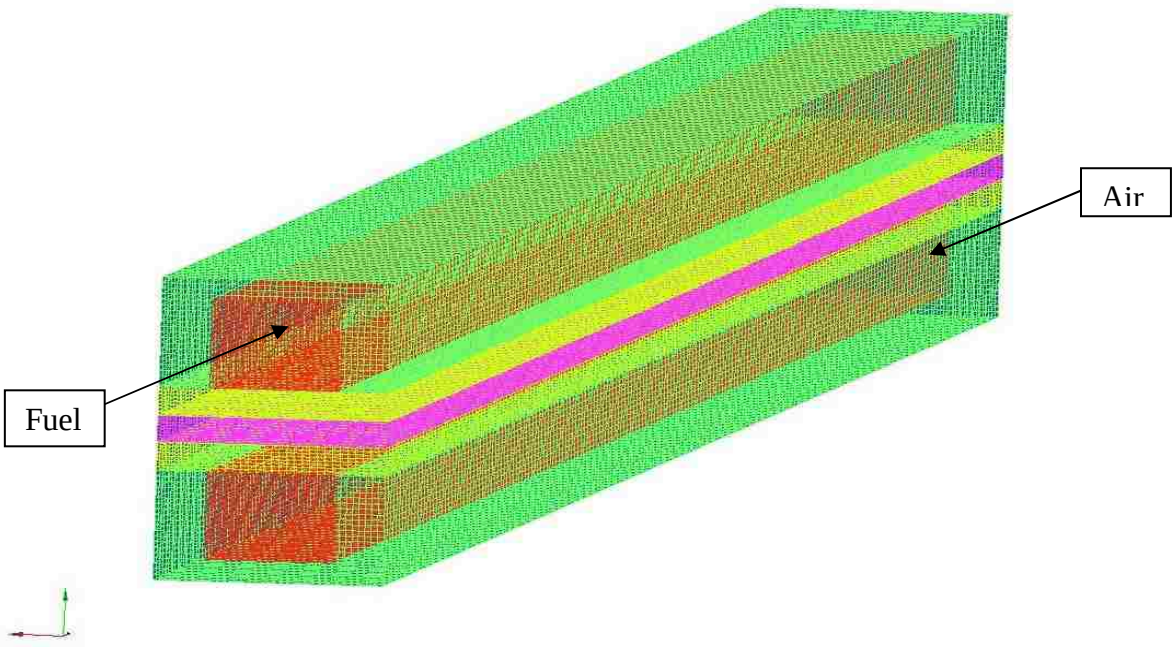

Fig 2.3 Computational mesh

Fig 2.3 shows the optimized computational mesh with 885,300 cells and 892,350 nodes which is created using the Hypermesh® software. The grid independent study will be discussed later. The mesh includes the nine zones which are mentioned above. The mesh with hexahedral elements is created. The heat transfer simulations are performed using the Fluent® software due to the memory problem encountered in the COMSOL® software. The electrochemical simulations are performed using the COMSOL® (FEMLAB) software.

2.2.2 Boundary Conditions

(1) Mass Inlet

In this present numerical model of single channel PEMFC there are two inlets hydrogen inlet (anode) and air inlet (cathode). A velocity inlet boundary condition is

given for both the inlets. The flow of hydrogen and air is in opposite directions. The mass flow rate at the anode is 6.0×10^{-7} kg/sec and the mass flow rate at the cathode is 5.0×10^{-6} kg/sec. The Reynolds number in the flow channel is 121.

The fuel is fed into the fuel cell as a mixture of gases. The gas mixture that is fed through the anode inlet consists of hydrogen and water vapor. The gas mixture that is fed through the cathode inlet consists of oxygen, water vapor and nitrogen. The mass fraction for hydrogen is set as 0.4 and the mass fraction for water vapor in the anode fuel mixture is set as 0.6. The mass fraction for oxygen is set as 0.15, the mass fraction of water vapor is set as 0.48 for water vapor and the mass fraction of the nitrogen is set as 0.37 at the cathode side.

(2) Thermal Boundary Conditions

The energy equation is solved to obtain the temperature distribution within the PEM fuel cell. Heat is generated due to the electrochemical reactions that are taking place at the surface of the catalyst layer and also due to the current flow in the membrane electrode assembly. The coupled heat transfer is solved between the fluid zones and the solid zones. The inlet fuel and air temperature are set as 323K, which is taken from the published data of Ticianelli et al. [8]. The side walls of the fuel cell are considered as adiabatic.

(3) Fluid Flow

The gas mixture is assumed as incompressible fluid. At the wall boundary, a non-slip boundary condition is assumed. The inlet mass flow rate of the gas mixture is taken from published data of Ticianelli et al. [8]. The outlet boundary condition is the pressure outlet with 0 Pa gauge pressure.

2.2.3 PEMFC Model

The single channel PEMFC model is modeled in COMSOL® software. Only half of the PEMFC single channel model is simulated as symmetric model to decrease the computational time because of the memory problem of COMSOL® software. There are many parameters which are should be given properly for simulation of the model. Different researchers used different sets of parameters depending upon the materials and operating conditions. To validate the PEMFC model, the parameters are properly set according to the physical properties in the experimental work done by Ticianelli et al. [8], the missing parameters from Ticianelli's work have been taken from the published work of Bernardi et al. [5]. The PEMFC parameters are listed in Table 2.2.

Table 2.2 PEMFC parameters

Parameter	Value
Anode ref. current density	5×10^{7} A/m^{2}
Anode ref. concentration	0.0564 kmol/m^{3}
Anode concentration exponent	0.5
Anode exchange coefficient	2

Cathode ref. current density	120 A/m^2
Cathode ref. concentration	3.39×10^{-3} $kmol/m^3$
Cathode concentration exponent	1
Exchange coefficient	1
Open-circuit voltage	1.15 V
Reference diffusivity hydrogen	9.15×10^{-5} m^2/s
Reference diffusivity oxygen	2.2×10^{-5} m^2/s
Reference diffusivity water	2.56×10^{-5} m^2/s
Reference diffusivity other species	3×10^{-5} m^2/s
Diffusion layer porosity	0.3
Diffusion layer viscous resistance	5.68×10^{12} $1/m^2$

Catalyst layer porosity	0.28
Catalyst layer viscous resistance	5.68×10^{12} $1/m^2$
Catalyst layer surface-to-volume ratio	200000 l/m
Membrane equivalent weight	1100 kg/kmol
MEA projected area	6.096×10^{-5} m^2
Absolute permeability K	1.76×10^{-11} m^2
Current collector/GDL/catalyst conductivity	120 S/m
Membrane conductivity	17 S/m
Current collector/GDL/catalyst thermal conductivity	150 W/m-K
Membrane thermal conductivity	0.95 W/m-K

2.2.4 Grid Independent Study

The grid independent study of the present numerical model is carried out by increasing the mesh density. The results are plotted and shown in Fig 2.4. When the mesh density is increased the numerical results of temperature reach a constant value. The fourth case in the plot is taken to be the grid independent model. The y-axis shows the temperature at cathode catalyst layer.

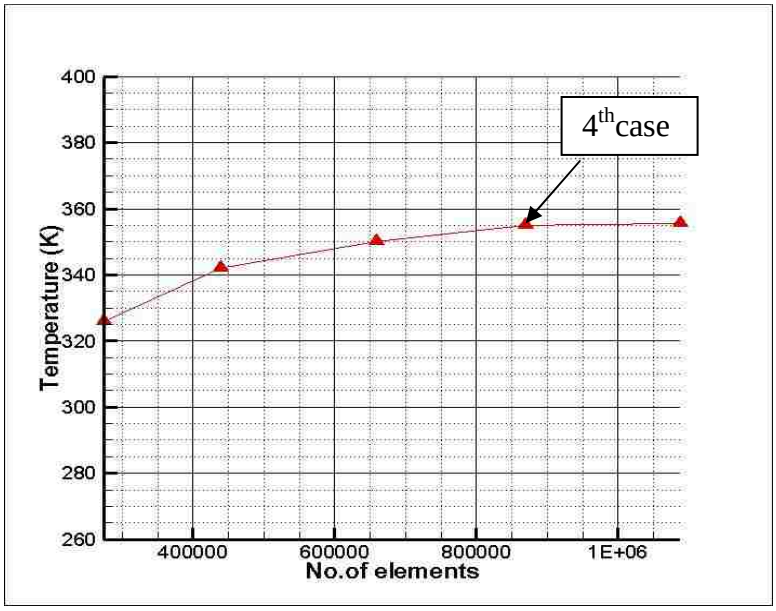

Fig 2.4 Grid independent study

2.2.5 PEMFC Model Validation

The single channel PEMFC model is numerically simulated using COMSOL® software using all the parameters show in Table 2.2. The j-V curve for the present model is generated and compared with the experimental results published by Ticianelli et al. [8]. Fig 2.5 shows the comparison of Ticianelli's results with the PEMFC numerical model

and the curves are very close to each other, therefore the present PEMFC model has been validated by Ticianelli's experimental work [8].

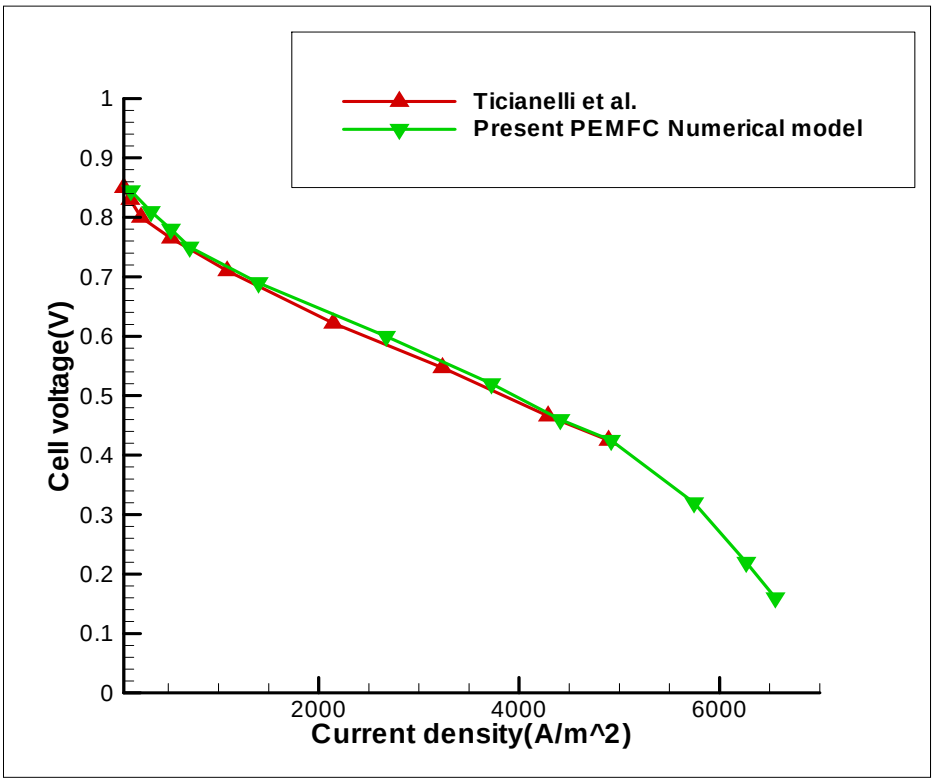

Fig 2.5 Comparison of the j-V curve of numerical model with experimental data

The hydrogen mass fraction, oxygen mass fraction and water mass fraction are shown in Figs 2.6, Fig 2.7 and Fig 2.8. From Fig 2.6 we can see that the hydrogen mass fraction decreases from inlet to outlet because the hydrogen is consumed as electrochemical reaction continues. From Fig 2.7 it can be seen that the oxygen mass fraction decreases from inlet to outlet because the oxygen is consumed as the electrochemical reaction takes place. From Fig 2.8 it can be seen that the water mass

fraction increases from inlet to outlet on the cathode side because water is produced from the electrochemical reaction.

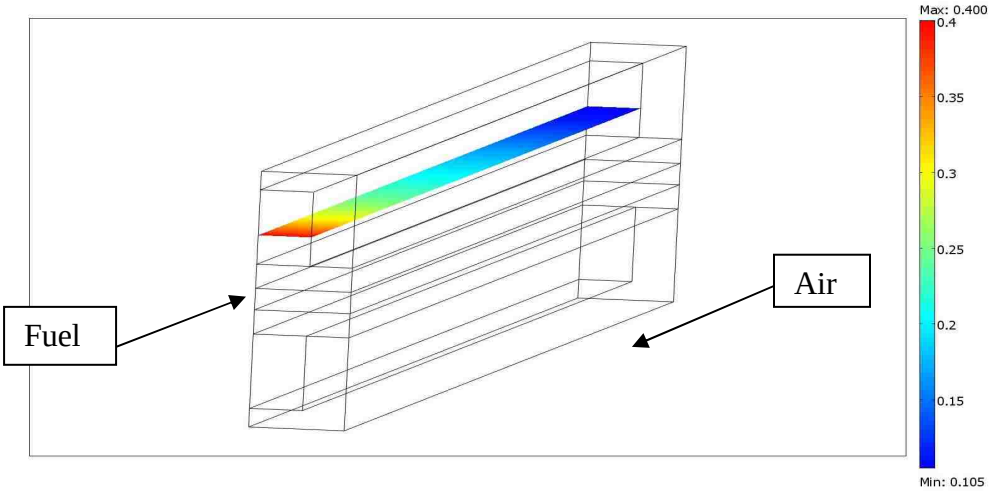

Fig 2.6 Hydrogen mass fraction at the anode side

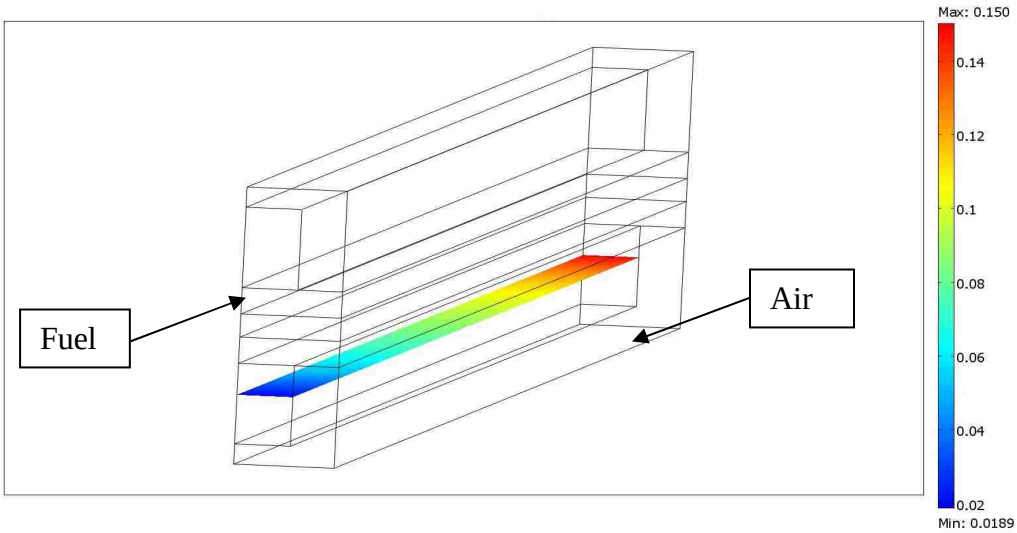

Fig 2.7 Oxygen mass fraction at the cathode side

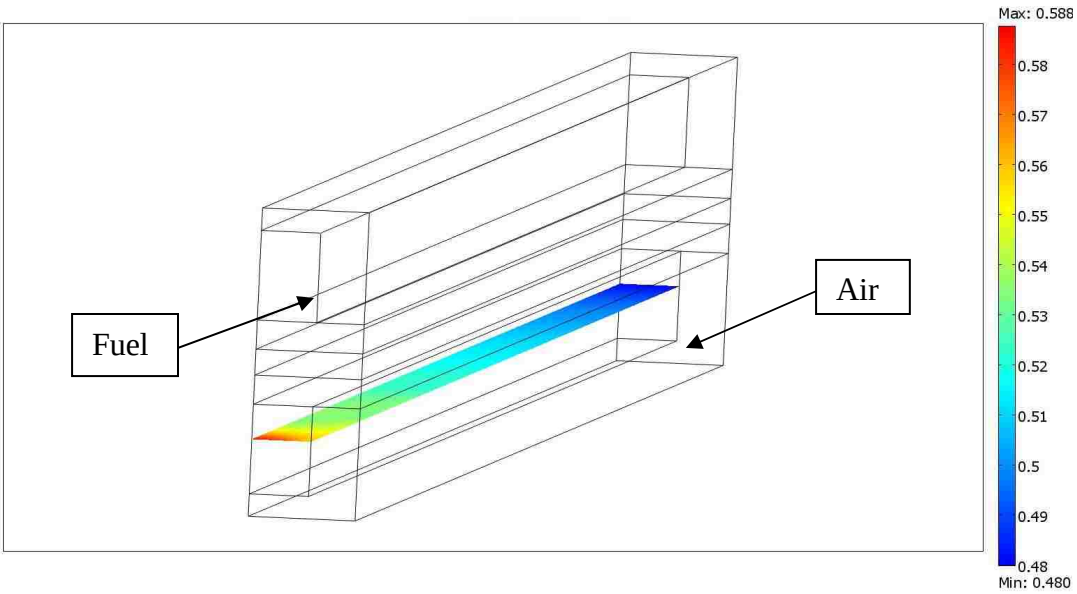

Fig 2.8 Water mass fraction at the cathode side

CHAPTER 3

DESIGN OF UNIFORM FLOW BIPOLAR PLATE

In this chapter the baseline design of the bipolar plate is taken, and a numerical analysis is carried out on it to study the velocity distributions. The flow distribution of the bipolar plate is very important because, if the flow distribution is non-homogeneous there will be a poor performance of the fuel cell and wastage of highly expensive catalyst. The flow distribution of the baseline design is found to be non-homogeneous. The design of the bipolar plate is changed to four inlets and four outlets so that the flow distribution becomes more homogeneous.

3.1 Design Description

The baseline design of the PEMFC is shown in Fig 3.1. The model consists of bipolar plates with thirteen channels each with one inlet and outlet. The whole model of the PEMFC consists of nine parts: two gas channels, two bipolar plates, two gas diffusion layers, two catalyst layers and a membrane. The parallel channel layout is implemented for the channels of the bipolar plate. The header section is designed with rectangular obstructions, so that the gases flow into the channels. The dimensions of the model are shown in Fig 3.2. The CAD model was designed using the commercial software SOLIDWORKS 2008®. The Initial Graphics Exchange Specification (IGES) file is loaded into Hypermesh® software for meshing of the designed CAD model.

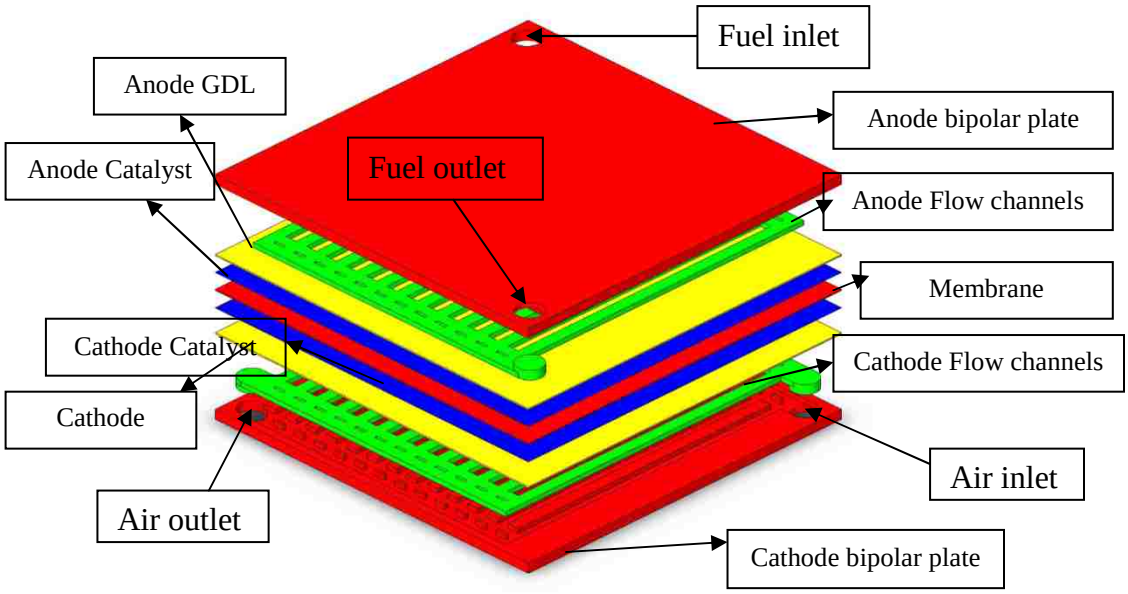

Fig 3.1 PEMFC baseline design

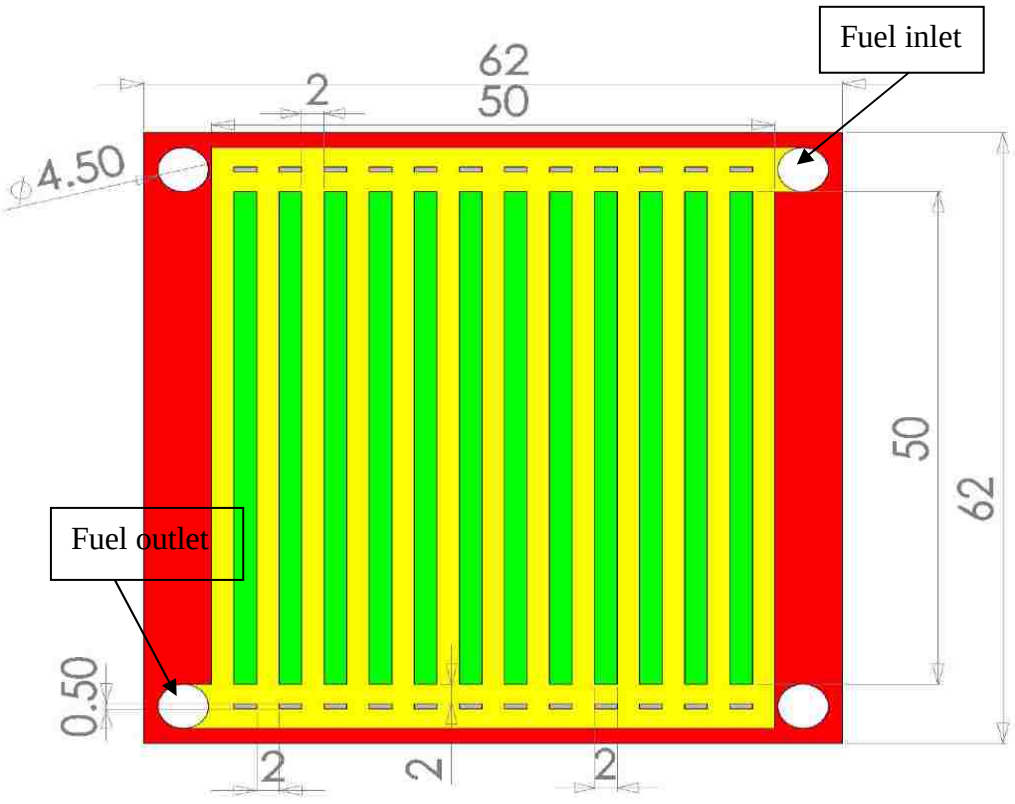

Fig 3.2 Dimensions of the baseline design of PEMFC (unit: mm)

The designed baseline design of the PEMFC consists of two bipolar plates with dimensions as shown in Fig 3.2. The thickness of the bipolar plate is 2 mm with 62 mm× 62 mm width and length. The channel width is 2 mm and the channel rib is 2 mm wide and 1 mm in height. The rectangular obstruction in the header area is 2 mm× 0.5 mm × 1 mm. The inlet diameter is 4.5 mm. The thickness of the gas diffusion layers is 0.26 mm. The thickness of membrane is 0.23 mm and the thickness of the catalyst layer is 0.01 mm. The gas diffusion layers, the catalyst layers and the membrane are 62 mm×62 mm in width and length. The computational mesh is generated by using the powerful meshing software Hypermesh ®. The generated mesh consists of 935,050 cells and 627,859 nodes which is the optimized one. The computational mesh can be seen in Figs 3.3(a), (b), (c). Hexahedral elements are used for the channels and tetrahedral elements are used at the inlet and outlet of the bipolar plate.

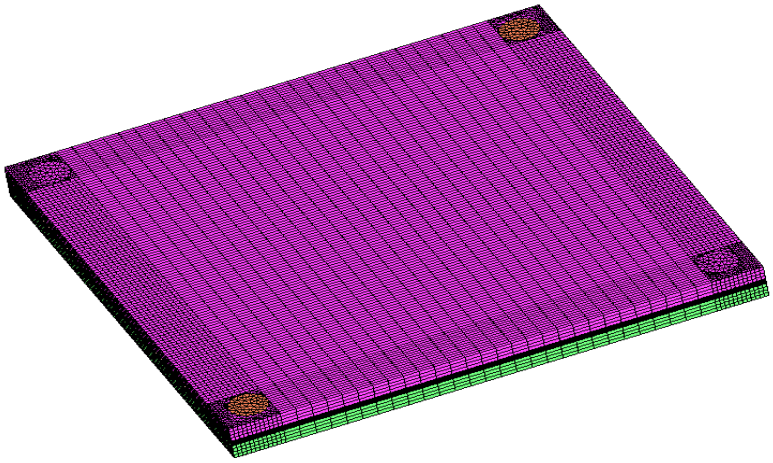

Fig 3.3(a) Computational mesh of the PEMFC

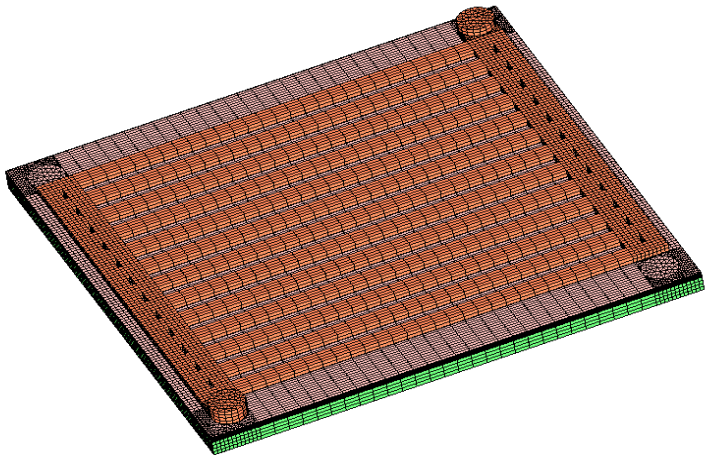

Fig 3.3(b) Computational mesh of channels and the MEA

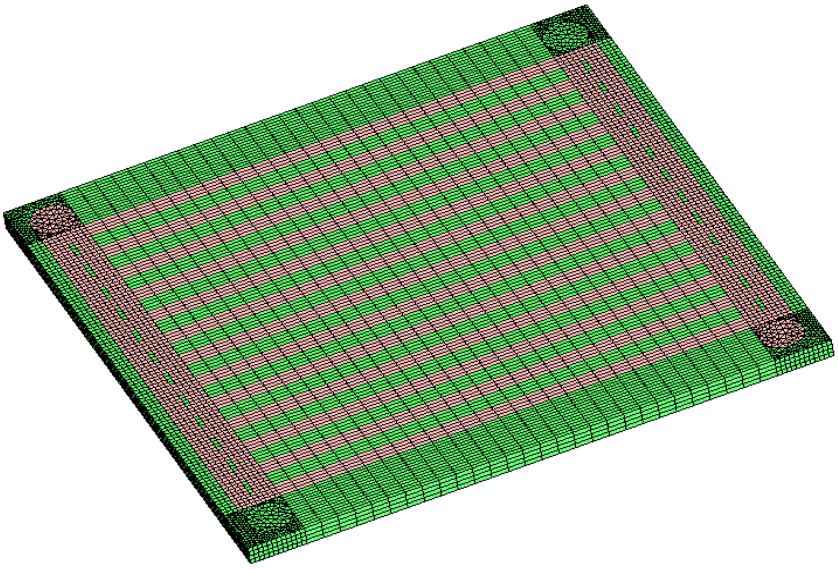

Fig 3.3(c) Mesh of bipolar plate and flow channels

3.2 Hydrodynamic Analysis

The commercial CFD software Fluent® is used as the computational tool for numerical analysis. Only a hydrodynamic analysis with no heat transfer is carried out on the above PEMFC and the electrochemical processes are not considered. The PEMFC module in Fluent is not available, so only the hydrodynamic analysis is carried out. The flow distributions in the bipolar plate are studied. The boundary conditions are: (1) anode mass inlet: 6.0×10^{-7} kg/sec, (2) cathode mass inlet: 5.0×10^{-6} kg/sec and the inlet temperature is given as 50^{o}C. The calculated result of flow distribution can be found in Fig 3.4. Fig 3.4 shows that the flow distribution is not uniform. The velocity is higher at the inlet and outlet and lower at the middle part of the bipolar plate. The bar chart below shows the flow distribution in the bipolar plate at the middle of the channel.

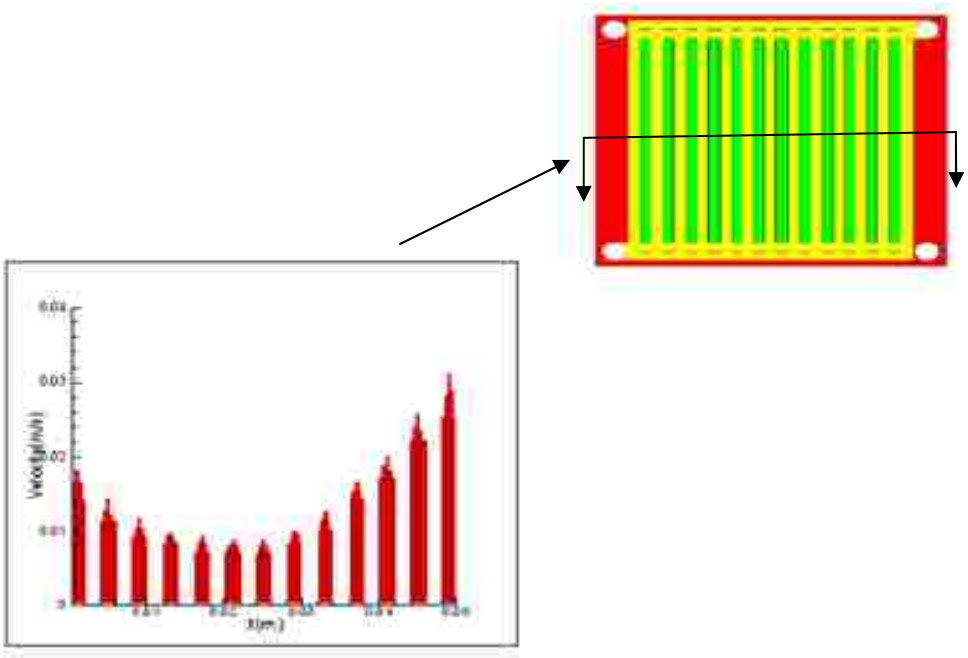

Fig 3.4 Flow distribution in the bipolar plate

The flow distribution in the baseline design of the bipolar plate is non-uniform and this leads to the wastage of very expensive catalyst and also there will be a poor performance of the fuel cell. The design of the bipolar plate should be changed, so that the flow distribution is uniform. The design of the bipolar plate is changed with four inlets and four outlets instead of one inlet and one outlet. The improved design of the PEMFC can be seen in Fig 3.5. The dimensions of the PEMFC can be found in Fig 3.6.

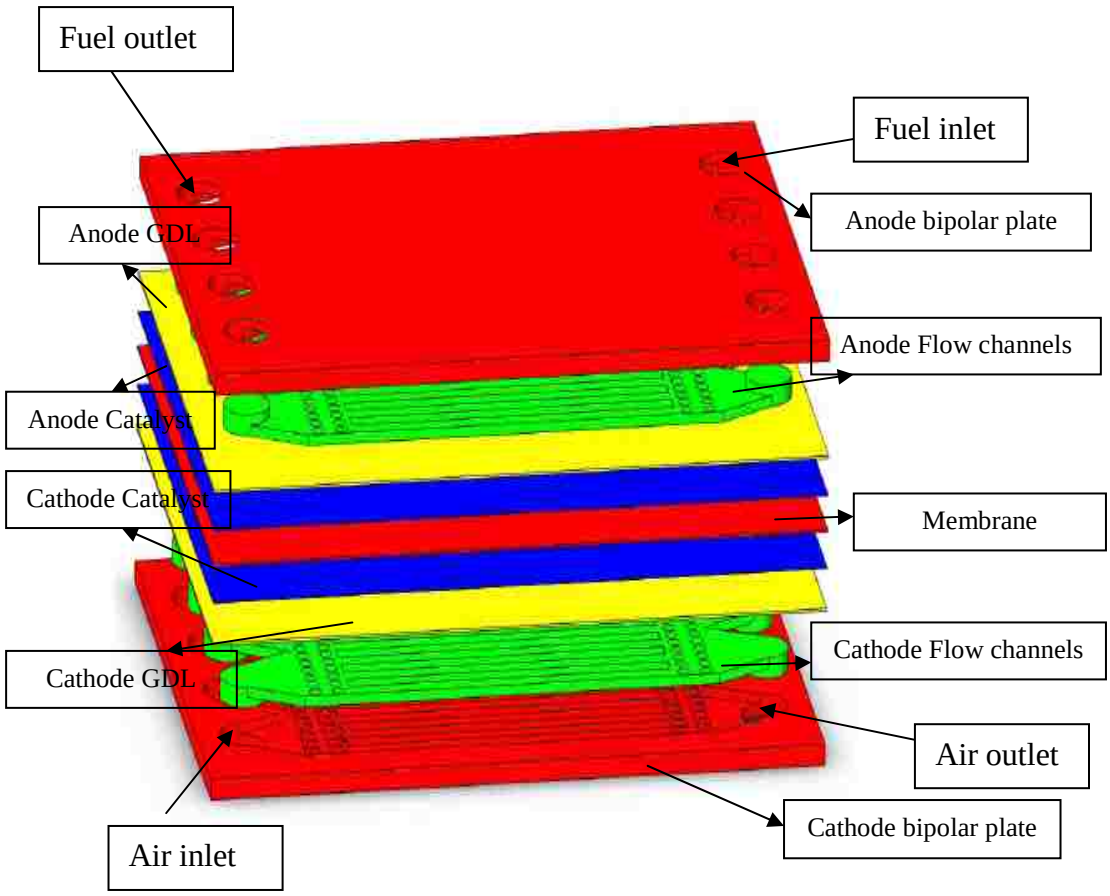

Fig 3.5 Improved design of PEMFC

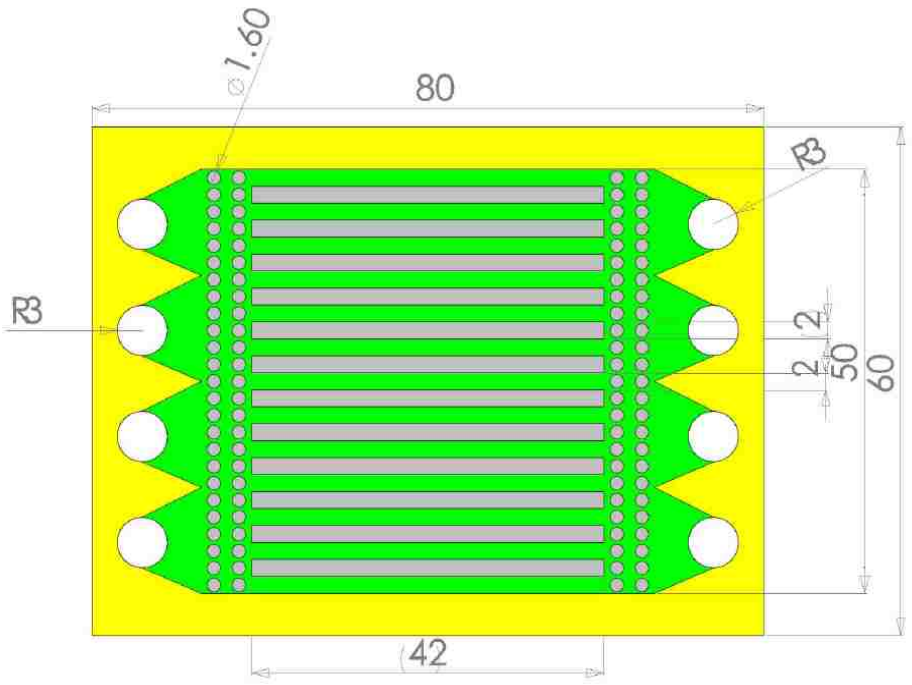

Fig 3.6 Dimensions of improved design PEMFC (unit: mm)

The dimensions can be seen clearly in Fig 3.6. The width of the bipolar plate is 60 mm and length 80 mm. There are four inlets and four outlets with 6 mm diameter each. The header is designed with cylindrical obstructions which are 1.6 mm in diameter and 1 mm in height. The channels present in the bipolar plate are 2 mm in width and 1 mm in height. The CAD model has been designed in the modeling software SOLIDWORKS 2008®. The IGES file was loaded into Hypermesh® software for meshing of the designed CAD model. Three-dimensional computational mesh is generated using Hypermesh® software. The computational mesh can be seen in Figs 3.7 (a), (b) and (c). The generated mesh consists of 1,587,586 elements and 858,736 nodes which is the optimized one. Hexahedral elements are used at the channels. Tetrahedral elements are used at the header, inlets and outlets. The boundary conditions are the same as the baseline design.

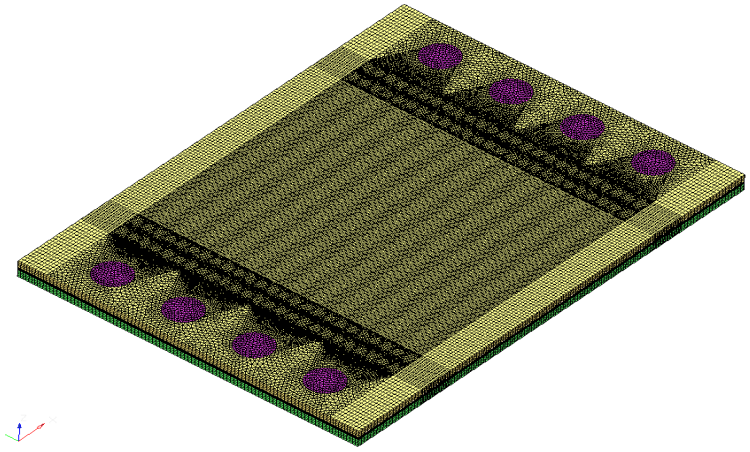

Fig 3.7(a) Computational mesh of improved design PEMFC

Fig 3.7(b) Computational mesh of flow channels and the MEA

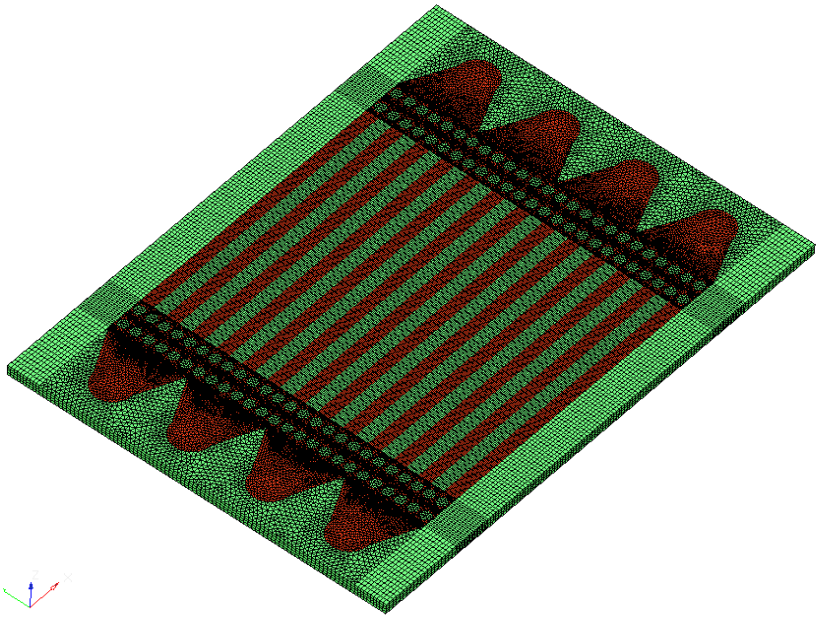

Fig 3.7(c) Mesh of bipolar plate and the channels

The CFD software Fluent® is used for numerical analysis of the PEMFC. Only hydrodynamic analysis is carried out on the present model. The electrochemical processes are not considered because the PEMFC module is not available in Fluent® software. The flow distributions are investigated inside the bipolar plate. The flow distributions inside the bipolar plate are seen in Fig 3.8. The flow distribution is almost uniform in every channel. The uniform flow is favorable for the fuel cell performance. The uniform flow distribution provides better adjustment of fuel supply which leads to higher efficiency of the fuel cell. The uniform flow distribution gives a uniform temperature distribution, uniform electrochemical reaction rate in catalyst layers, and efficient usage of expensive catalyst.

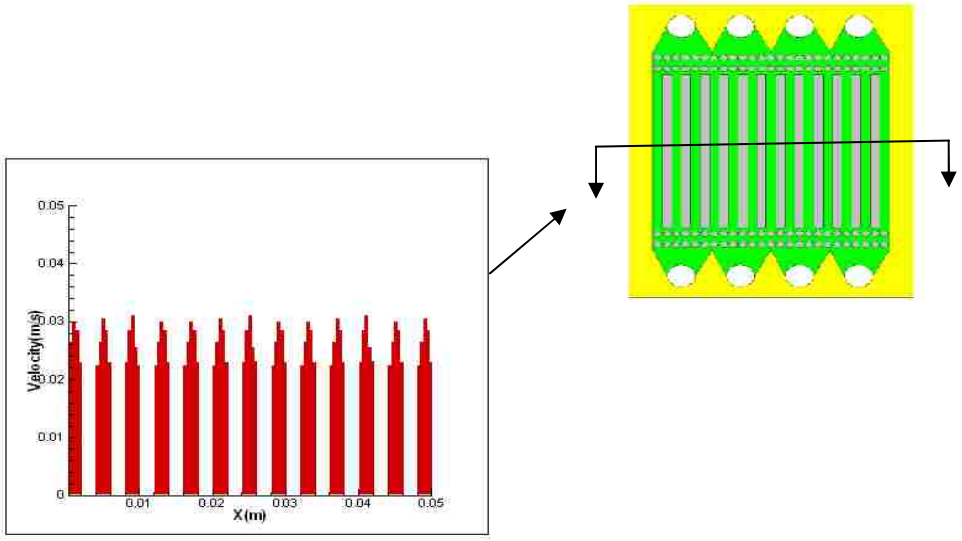

Fig 3.8 Flow distribution inside the channels of the improved design of PEMFC

The flow distribution is very uniform in the channels of the bipolar plate. One of the channels is taken to carry out the electrochemical analysis. COMSOL MULTIPHYSICS 3.5a is used for electrochemical analysis. Due to the limitation on the extensive memory requirement of COMSOL®, only a single channel shown in Fig 3.9 is selected to simulate the behavior of the PEMFC. The same problem is faced by Xing et al. [34], and the same thing was done by them. The half of the single channel of the improved design PEMFC is taken and run as a symmetric model and the electrochemical analysis is carried out. Fig 3.10 shows the temperature distribution along the cathode gas channel. Fig 3.11 shows the temperature distribution along the anode gas channel. From Figs 3.10 and 3.11 we can observe that the outlet temperature at cathode is more than that of the anode because the electrochemical reaction produces exothermic heat which is absorbed by the air at the cathode side. The heat from the cathode is absorbed by the anode also by conduction.

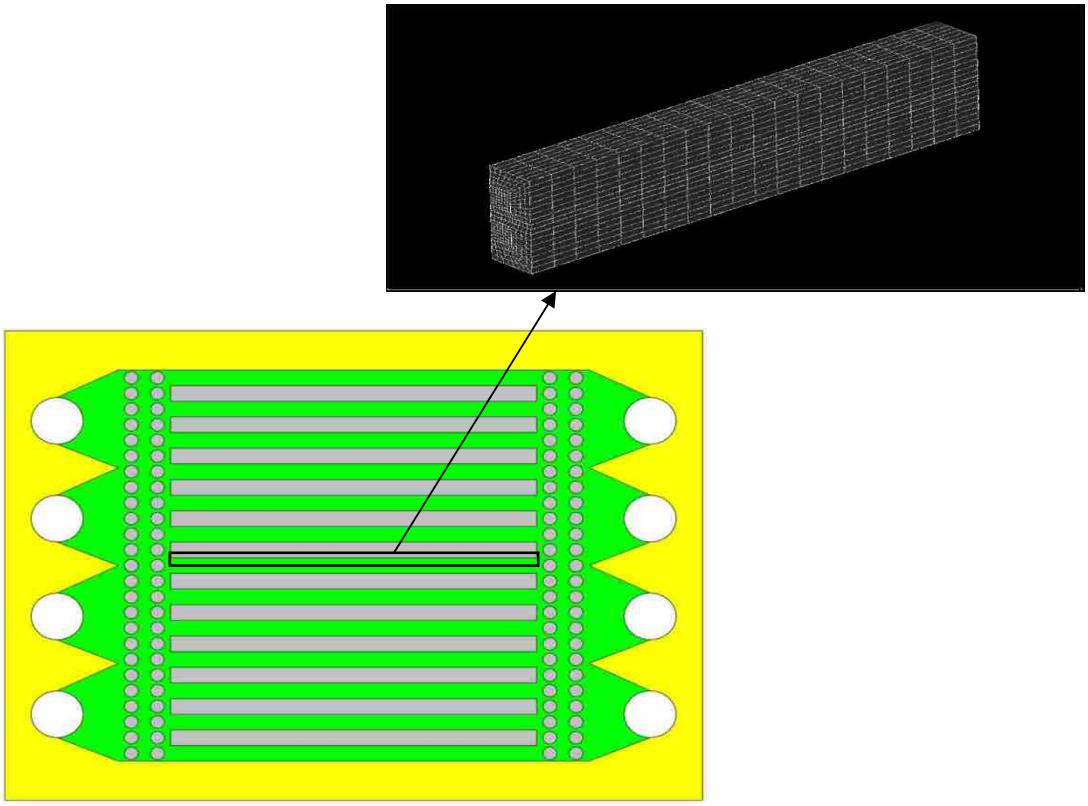

Fig 3.9 Computational domain

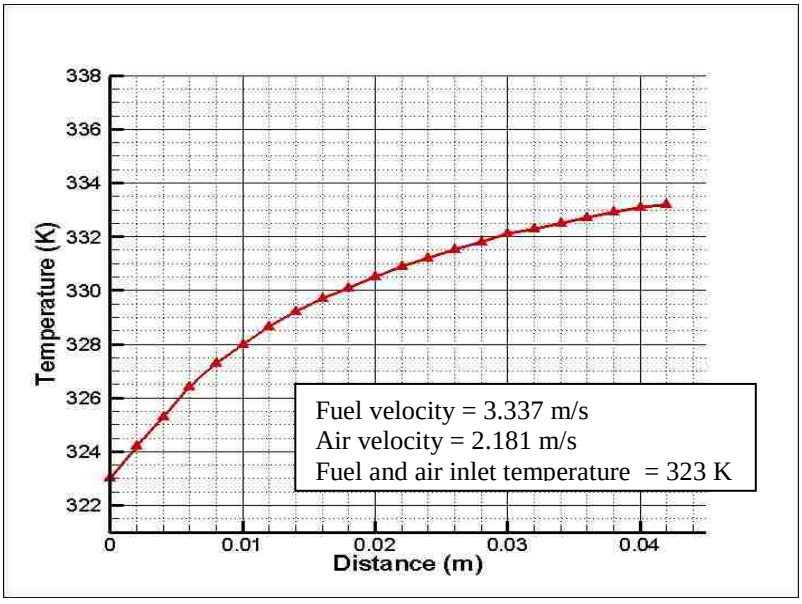

Fig 3.10 Temperature distribution along the cathode gas channel

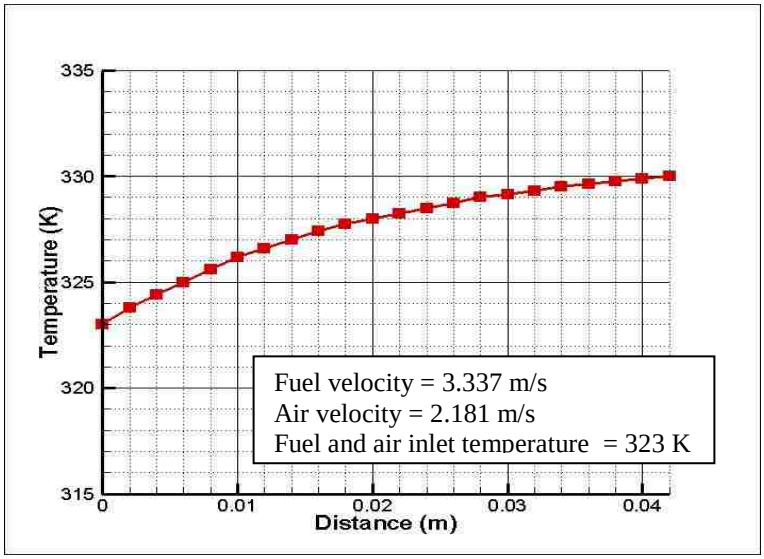

Fig 3.11 Temperature distribution along the anode gas channel

3.3 Electrochemical Analysis

The electrochemical analysis is carried out using COMSOL MULTIPHYSICS 3.5a software and the mass fractions of hydrogen, oxygen and water at the anode and cathode are shown in Figs 3.12, 3.13and 3.14. From Fig 3.12 we can observe that the hydrogen mass fraction decreases from inlet to outlet at the anode channel. From Fig 3.13 it is seen that the oxygen mass fraction is decreased from inlet to outlet at the cathode channel. From Fig 3.14 it can be seen that the water mass fraction increases from inlet to outlet.

The mass fraction of hydrogen decreases from inlet to the outlet because hydrogen is consumed by the electrochemical reaction along the length of the channel. The mass fraction of oxygen decreases from inlet to outlet because the oxygen is used up by the electrochemical reaction to produce electricity. The water mass fraction increases from inlet to the outlet because the hydrogen and oxygen ions combine and form by-product water which is produced at the cathode channel of the PEMFC.

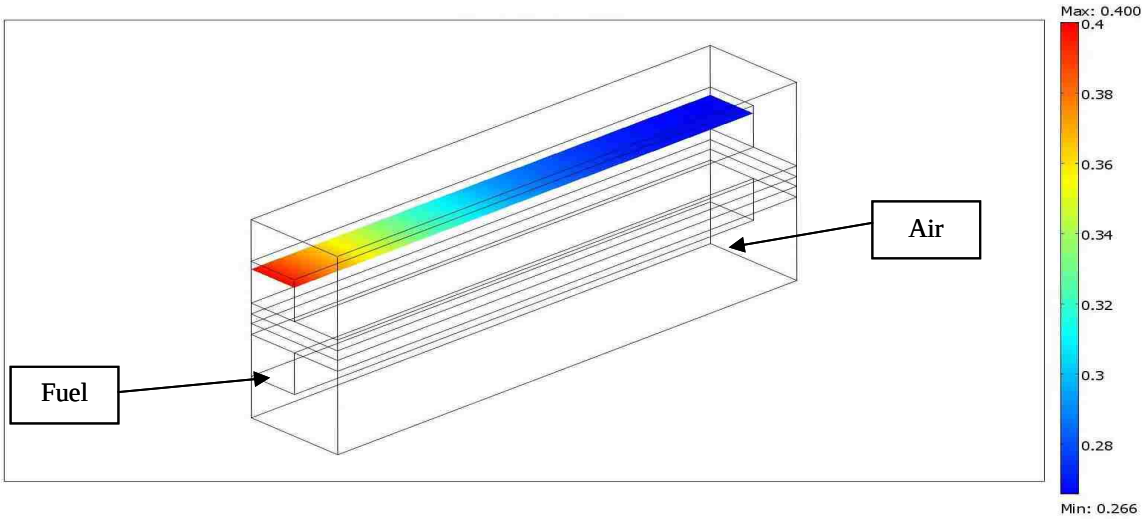

Fig 3.12 Hydrogen mass fraction at the anode channel

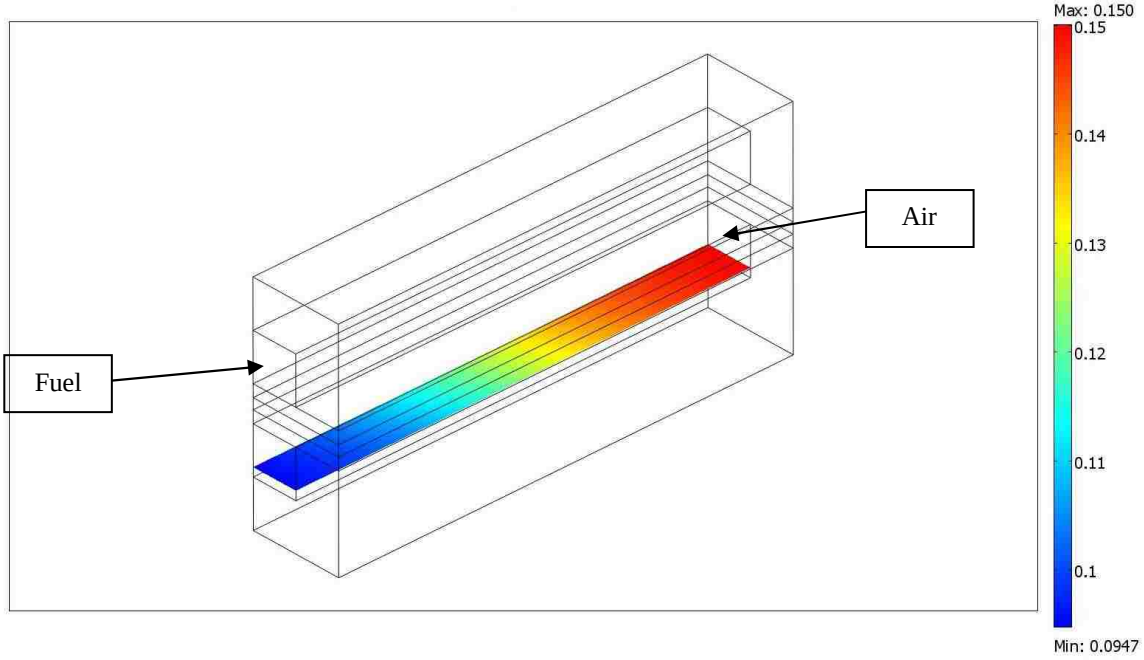

Fig 3.13 Oxygen mass fraction at the cathode gas channel

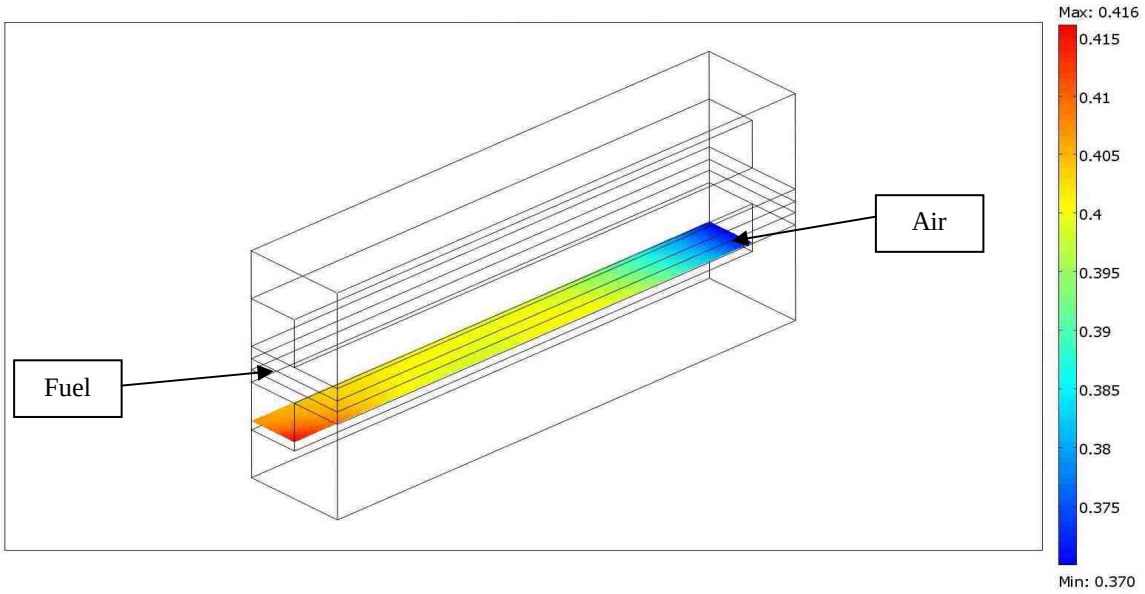

Fig 3.14 Water mass fraction at the cathode gas channel

CHAPTER 4

OPTIMIZATION OF PEMFC CHANNEL GEOMETRY

In this chapter the geometry of the channel is changed from rectangular to square, semi-circle and triangle, and the performances are determined. From the obtained numerical results it is seen that the rectangular geometry is better than all of the geometries. The triangular channel has the poorest performance of all the four channel geometries. The numerical results for different geometries are found for various temperatures and pressures.

4.1 Design Description

The geometry of the channel has been changed to different shapes. The shape of the channel designed in Chapter 3 is rectangular. The shape of the channel is changed from rectangular to square, semi-circle and triangular shapes. The shapes of the channels can be seen in Figs 4.1, 4.2, 4.3 and 4.4. The width of the rectangular channel is 2 mm and height is 1 mm.

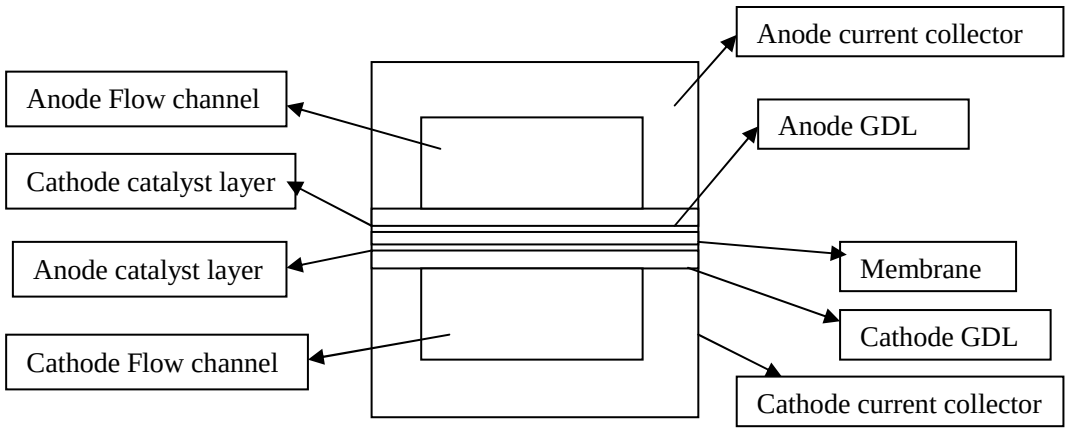

Fig 4.1 Rectangular channel

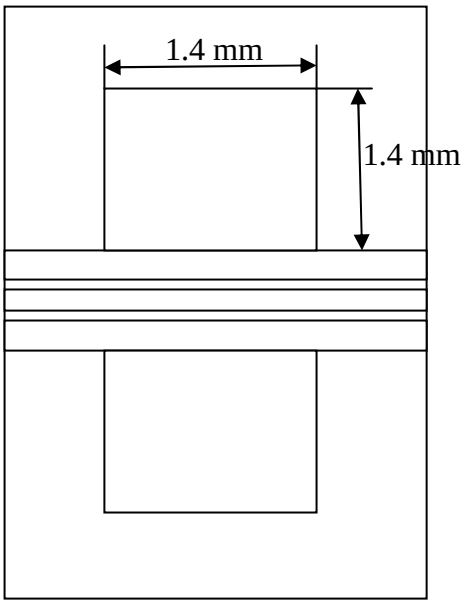

Fig 4.2 Square channel

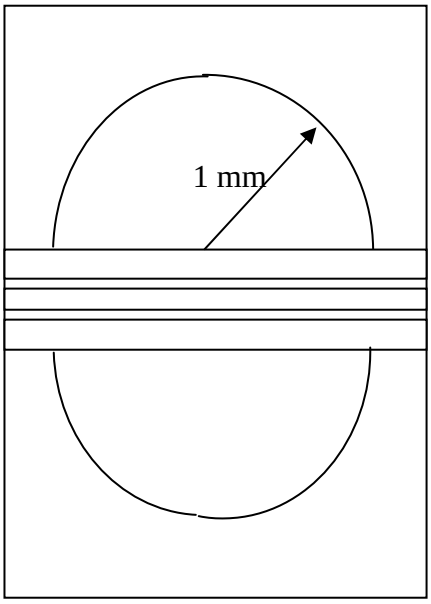

Fig 4.3 Semi-circular channel

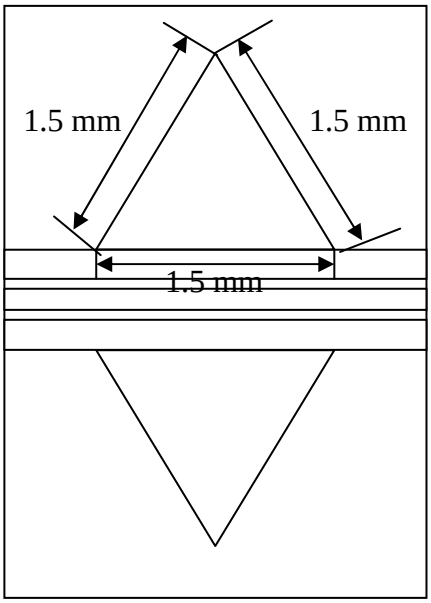

Fig 4.4 Triangular channel

4.2 Numerical Analysis

The COMSOL MULTIPHYSICS 3.5a is used for electrochemical analysis of all the channel geometries. The parameters and boundary conditions stated in Chapter 2 are used for the numerical analysis. The rectangular, square, semi-circular and triangular channels are numerically simulated and a j-V curve is plotted for each. The j-V curves can be seen in Fig 4.5. From Fig 4.5 it can be observed that rectangular channel shows better performance than that of every other channel. The performance of the rectangular is 6.3% greater than the triangular channel.

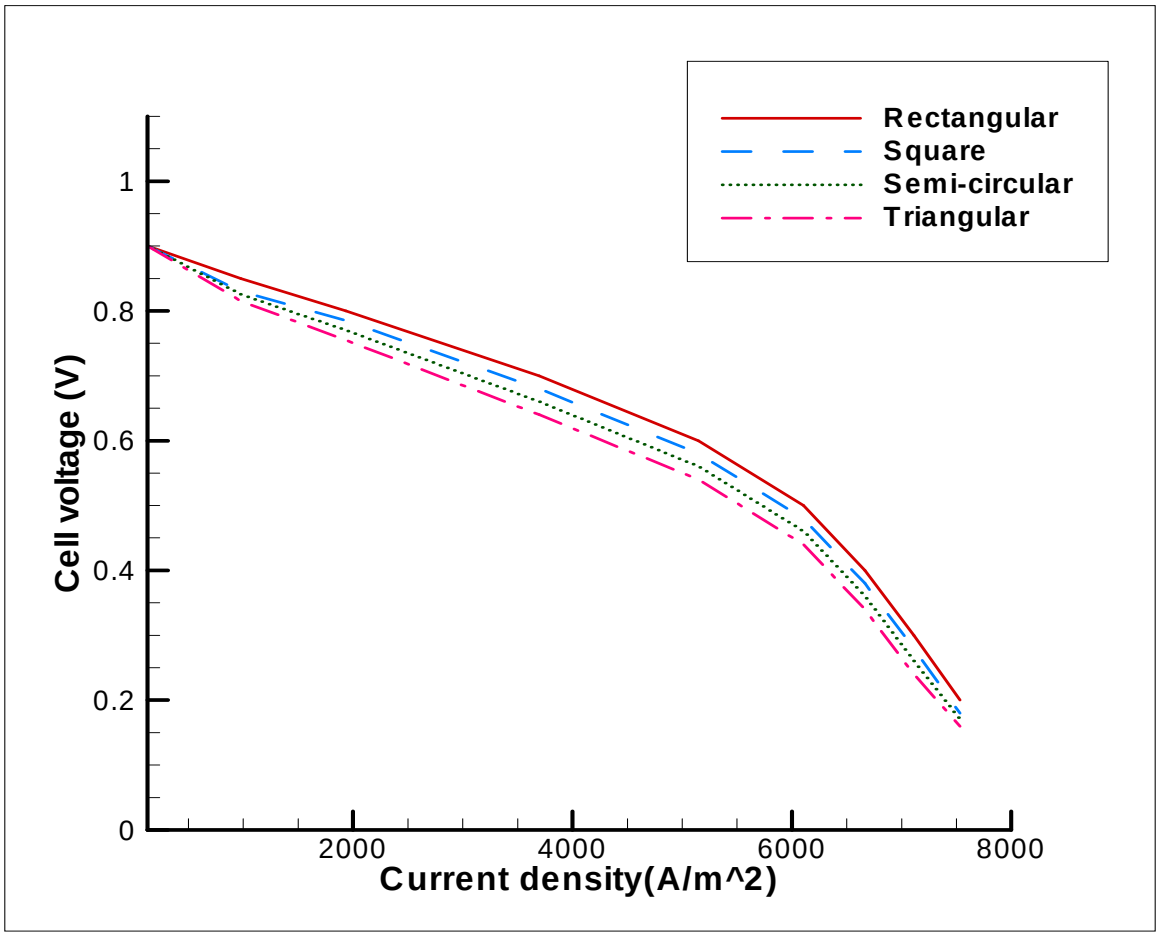

Fig 4.5 j-V curves of different channel geometries

The reason for the above behavior may be due to the area surrounding the channel. The area surrounding the channel is determined and compared with the performance. The area of the solid surface in contact with the fluid flow influences the performance of the fuel cell. The larger the area the higher is the performance. The total channel surface areas are: rectangular channel 240 mm^2, square channel 224 mm^2, semi-circular channel 205.6 mm^2, triangular channel 180 mm^2. The rectangular channel has the larger area when compared with other channels, so the performance of the rectangular channel is better than all the channels. The current produced is directly proportional to

the area of interface [2]. Doubling the interfacial area available for the reaction should double the rate of the reaction. The large area has better reaction rate, so there is an increase in performance when the area is increased. The current density (current per unit area) is more fundamental than current. The current density allows the reactivity of different surfaces to be compared on a per-unit basis. Current density j is expressed in units of amperes per square centimeter (A/m^2):

$$j = \frac{i}{A} \tag{4-1}$$

where A is the area and i is the current (A)

In a similar fashion, the electrochemical reaction rates are also expressed on a per-unit area basis. The per-unit area reaction rate is given the symbol J. Area-normalized reaction rates are usually expressed in units of moles per square centimeter per time ($mol/cm^2/s$):

$$J = \frac{1}{A}\frac{dN}{dt} = \frac{i}{nFA} = \frac{j}{nF} \tag{4-2}$$

where F is the Faraday's constant , A is the area and n is the number of moles of electrons transferred during the electrochemical reaction. The above equations show the importance of the area. The larger area is better for reactions. The main parameter, current density, is related to area. Fig 4.6 shows the power density curves of different channel geometries. The power density curves show that the maximum power is obtained at a voltage of 0.6 V. The power density obtained from the rectangular channel is better than all the channels.

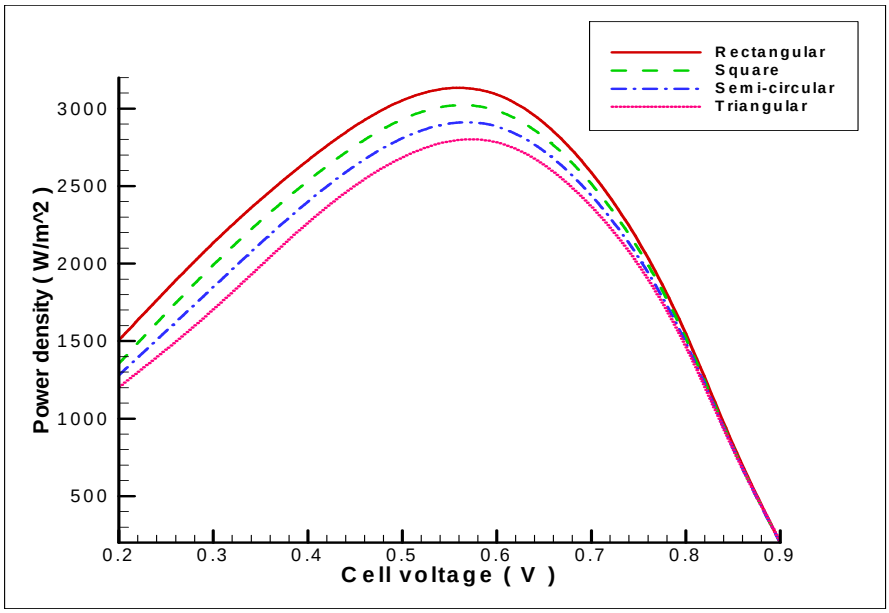

Fig 4.6 Power density curves of different channel geometries

4.3 Pressure Drop Calculation

The pressure drop is very important in the design of channels. The pressure difference between the inlet and outlet drives the fluid flow. Increasing the pressure drop between the inlet and outlet will increase the mean gas velocity in the channel, improving convection. The pressure drop is calculated analytically for different channels and compared with the numerical results obtained. For circular flow channels, the relationship between pressure drop and mean gas velocity may be calculated from the relation [2]

$$\frac{dp}{dx} = \frac{4}{D}\tau_w \tag{4-3}$$

where dp/dx is the pressure gradient, D is the flow channel diameter, and the mean wall shear stress τ_w may be calculated from a nondimensionalized number called the friction factor,f [2]:

$$f = \frac{\tau_w}{1/2\rho u^2} \tag{4-4}$$

where ρ is the fluid density (kg/m^3) and u is the mean flow velocity (m/s). It is found that regardless of channel size or flow velocity, fRe = 16 for laminar flow in circular channels. Furthermore, for circular channels [2]

$$Re = \frac{\rho u D}{\mu} \tag{4-5}$$

Thus, by combining equations (4-3), (4-4) and (4-5) and the fact that fRe = 16, the pressure drop and mean gas velocity may be related:

$$\frac{dp}{dx} = \frac{32u}{D^2} \tag{4-6}$$

Unfortunately, most fuel cell flow channels are rectangular instead of circular. For rectangular channels equation (4-6) cannot be used. For rectangular channels, we must use hydraulic diameter to compute the effective Reynolds number compared to a circular channel [2]:

$$Re_h = \frac{\rho u D_h}{\mu} \tag{4-7}$$

where

$$D_h = \frac{4A}{P} = \frac{4 \times cross\text{-}sectional\ area}{perimeter} \tag{4-8}$$

For rectangular channels, the relationship between Re_h, and f is more complex than for circular channels. It can be approximated as [35]:

$$fRe_h = 24(1 - 1.355\alpha^* + 1.9467\alpha^{*2} - 1.7012\alpha^{*3} + 0.9564\alpha^{*4} - 0.2537\alpha^{*5}) \tag{4-9}$$

where α^* is the aspect ratio of the channel cross section: $\alpha^* = b/a$, where 2 a and 2 b are the lengths of the channel sides. The aspect ratio α^* for different channel geometries can be obtained as shown in Fig 4.7.

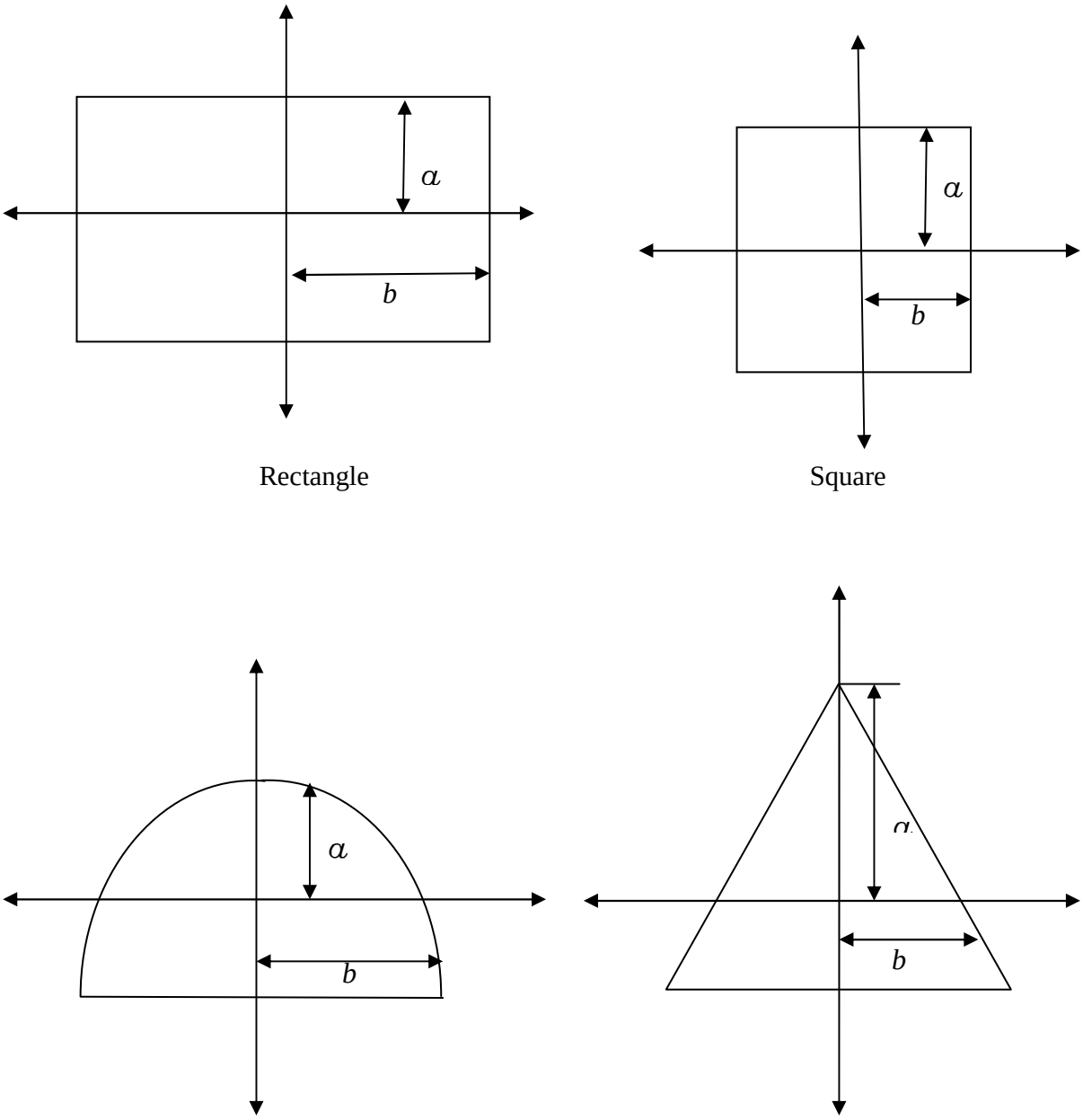

Fig 4.7 Aspect ratio calculation for different geometries

The pressure drop in the channels is calculated analytically and compared with the numerical results in Table 4.1. The numerical results approached the analytical value with less than 5% error. The analytical calculations are carried out considering the flow in the channel as fully developed, so the numerical results are overestimated compared to analytical values.

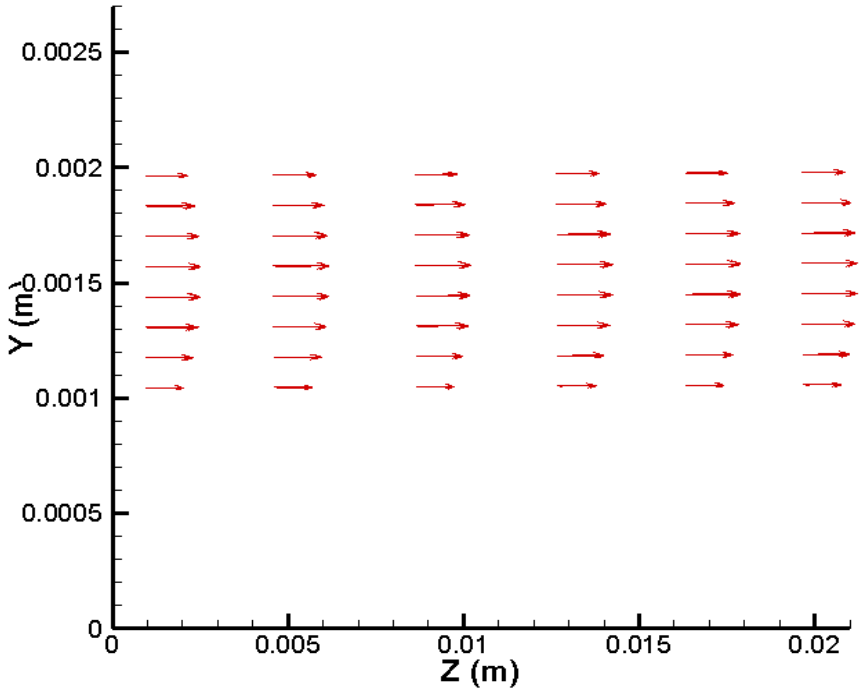

Fig 4.8 Velocity vector plot in the gas channel

Fig 4.8 shows that the flow inside the channel is not fully developed. The developing lengths on the anode side and cathode side are found to be 39.29 mm and 37.89 mm. The length of the channel should be increased to a length greater than the developing length.

Table 4.1 Pressure drop comparison

Type of geometry	Pressure drop (Pa)		
	Analytical value	Numerical results	Error (%)
Rectangular	132.3	138.65	4.58
Square	107.04	111.62	4.10
Semi-circle	145.68	151.36	3.75
Triangle	155.42	162.63	4.43

4.4 Temperature Variation

The operating temperature is changed from 323K to 338K and 353K and the performance of the fuel cell is observed. The pressure on the cathode and anode side is 1 atm. The performance of the fuel cell increases with increase in temperature. The reason behind this nature is that the kinetic performance focuses on increasing j_0 (exchange current density). To understand how j_0 is increased we have to take a look how j_0 is defined. The j_0 is defined by the equation (4-8) [2].

$$j_0 = nFC_R^* f_1 e^{-\Delta G_1/(RT)} \tag{4-8}$$

where j_0 is the exchange current density, F is Faraday's constant, n is the number of moles of electrons, C_R^* is the reactant concentration, ΔG_1 is the activation barrier and T is the temperature.

From the above equation we can observe that by increasing the temperature the exchange current density can be increased, and thereby increasing the performance of the fuel cell. By increasing the reaction temperature, we are increasing the thermal energy available in the system. When the thermal energy in the system is increased all particles in the system move about and vibrate with increased intensity. The higher level of thermal activity increases the likelihood that given reactants will posses sufficient energy to reach the activated state, thus increasing the rate of reaction [2]. Changing the temperature has an exponential effect on j_0. The j-V curves for the various channel geometries at different temperatures are presented in Figs 4.9, 4.11, 4.13 and 4.15. The power density curves are presented in Figs 4.10, 4.12, 4.14, 4.16.

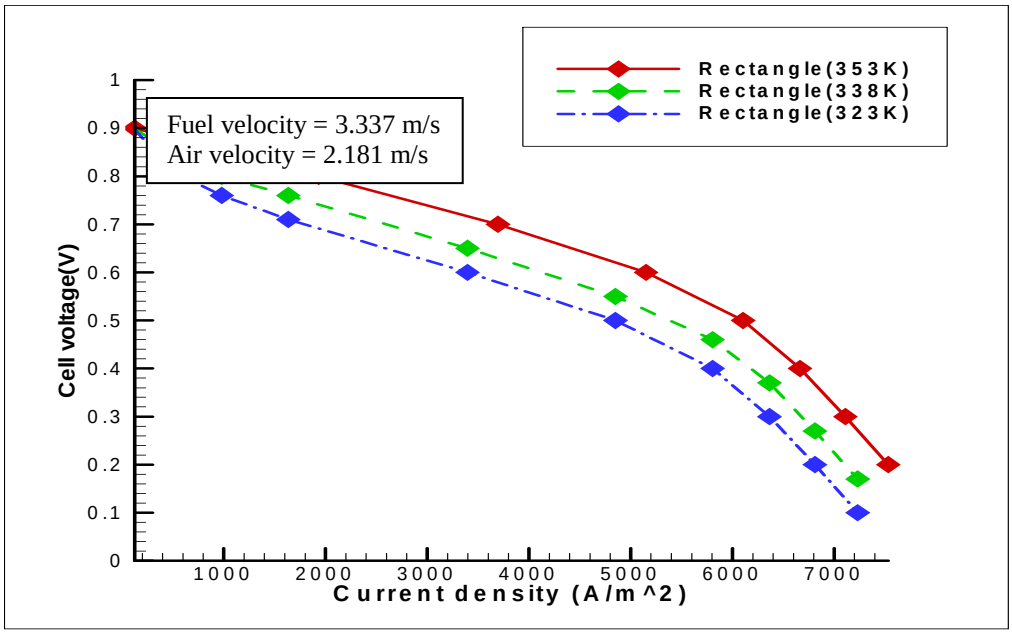

Fig 4.9 j-V curves of the rectangular channel at different temperatures

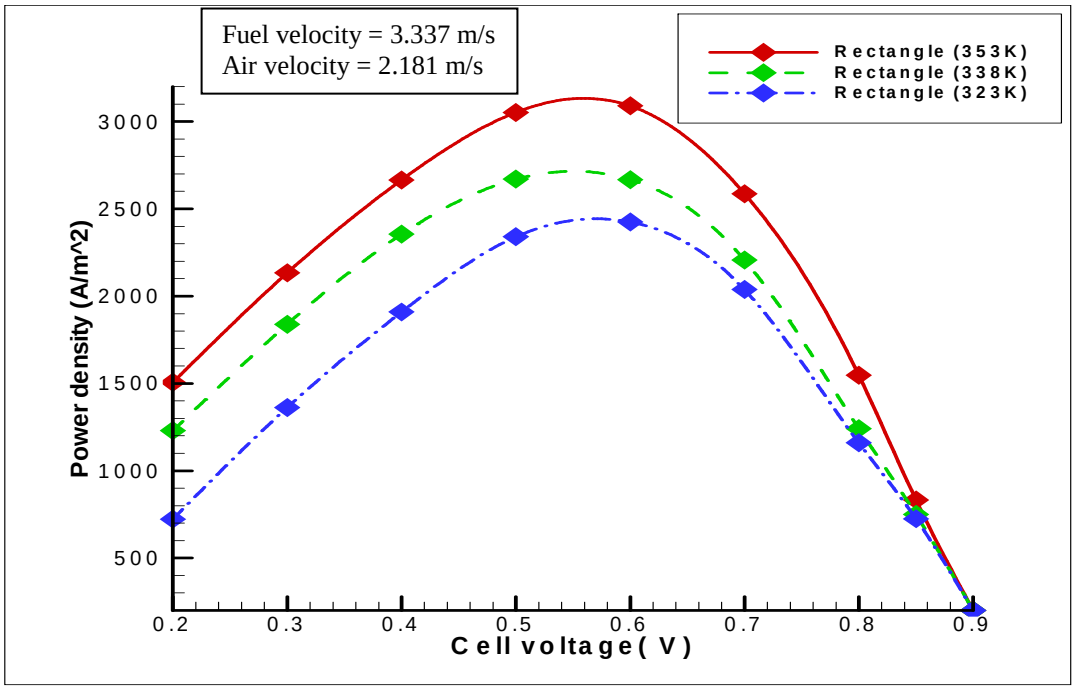

Fig 4.10 Power density curves of the rectangular channel at different temperatures

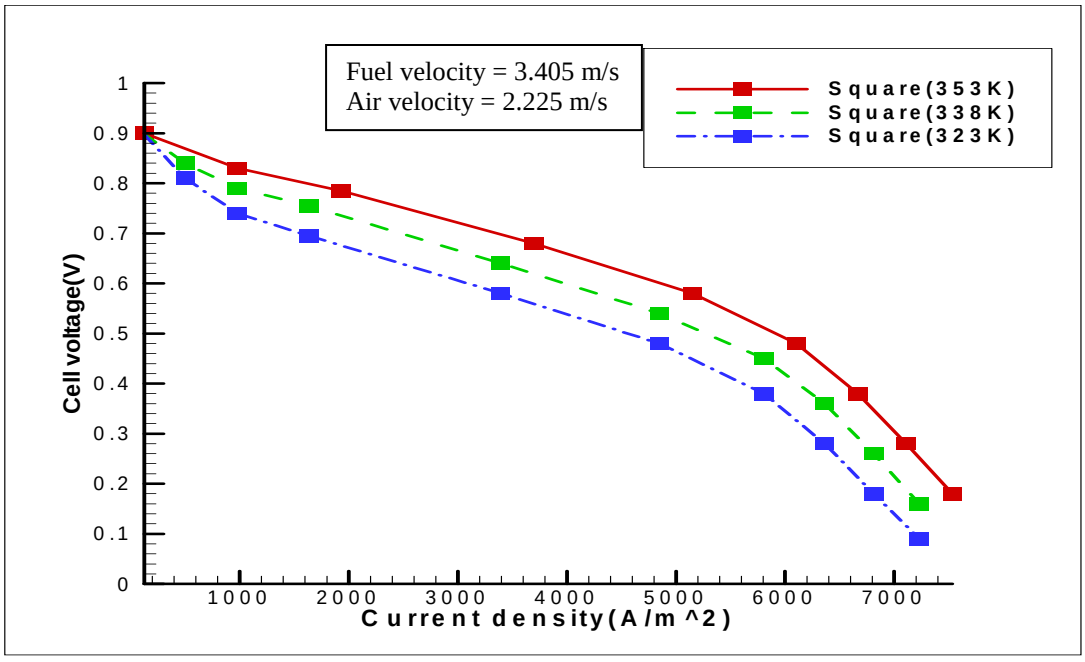

Fig 4.11 j-V curves of the square channel at different temperatures

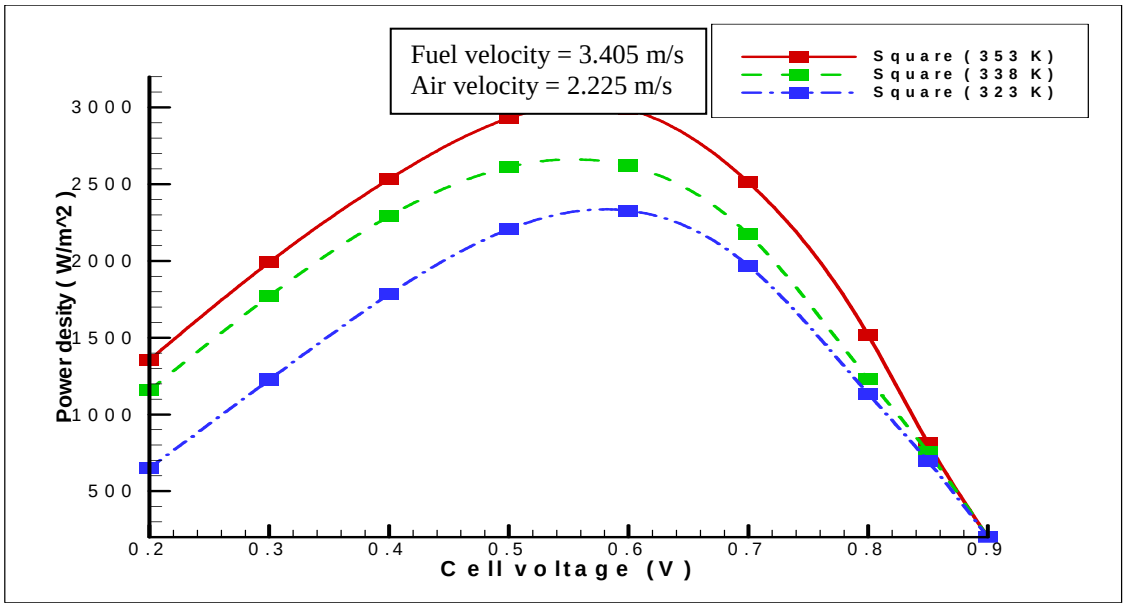

Fig 4.12 Power density curves of the square channel at different temperatures

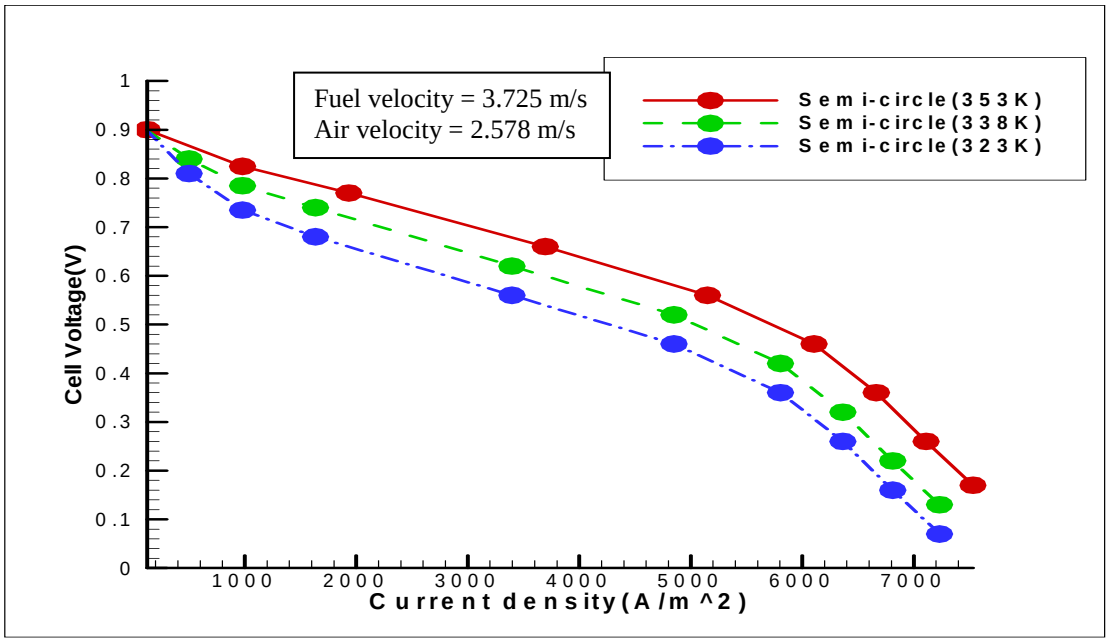

Fig 4.13 j-V curves of the semi-circular channel at different temperatures

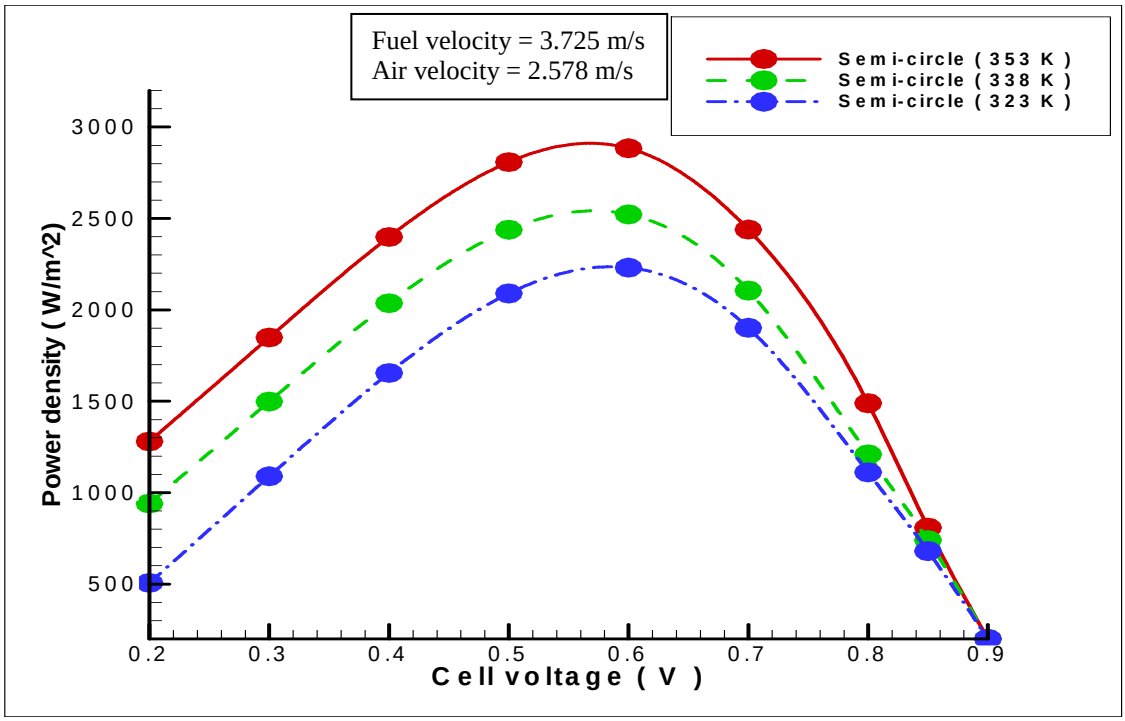

Fig 4.14 Power density curves of the semi-circular channel at different temperatures

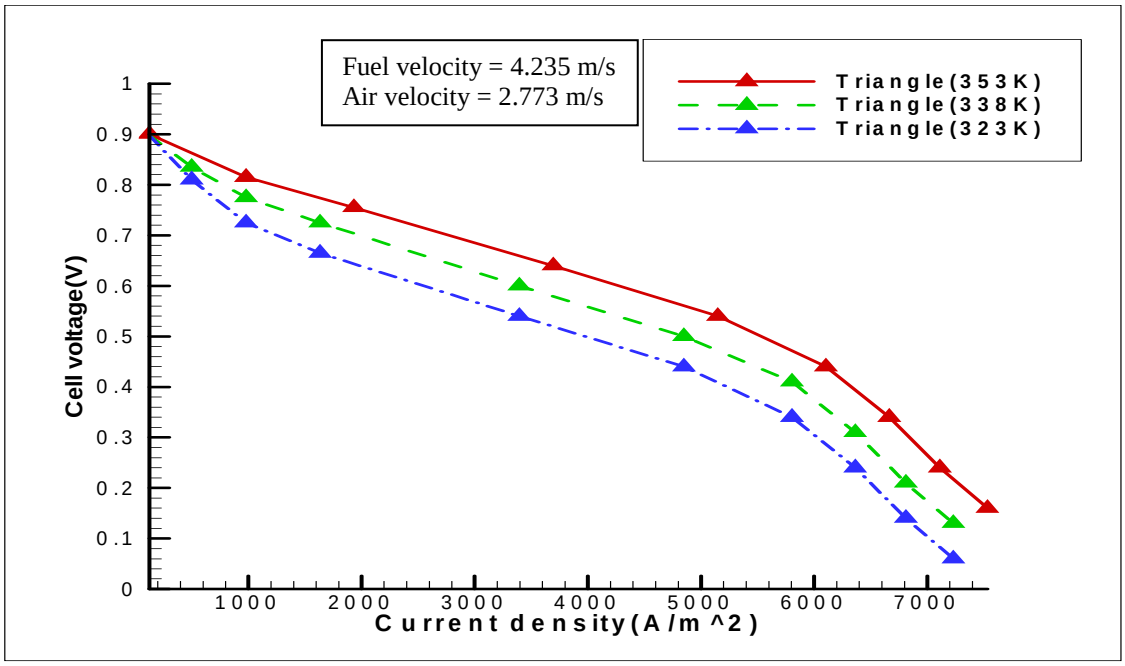

Fig 4.15 j-V curves of the triangular channel at different temperatures

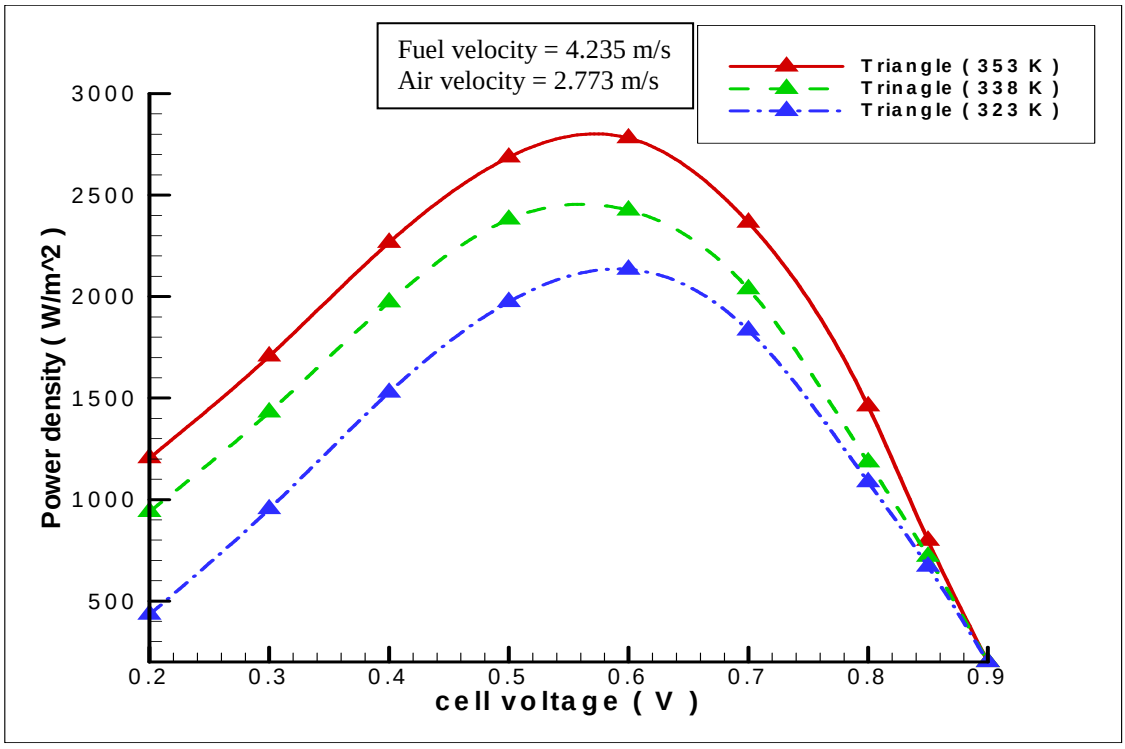

Fig 4.16 Power density curves of the triangular channel at different temperatures

From the above Figs 4.9, 4.11, 4.13 and 4.15 we can observe that the slope of the j-V curve changes with variation of temperature at the activation region. The slope of the j-V curve doesn't change in the ohmic region and in the concentration region. This is because increase in temperature influences only the activation as explained above and doesn't influence the ohmic and concentration regions of the j-V curve. The slopes of the above j-V curves are tabulated in Table 4.2. The solid line in Figs 4.9, 4.11, 4.13 and 4.15 represents the j-V curve at 353K (80^0C), the dashed line in Figs 4.9, 4.11, 4.13 and 4.15 represents the j-V curve at 338K (65^0C) and the dashed dot line in Figs 4.9, 4.11, 4.13 and 4.15 represents the j-V curve at 323K (50^0C).

Table 4.2 Slopes of the j-V curves at different temperatures

Shape of the channel	Temperatures (1)353K, (2)338K and (3)323K Slope			
	Activation region (400 – 1000 A/m^2)		Ohmic region (2000 – 4200 A/m^2)	Concentration region (5500 – 6400 A/m^2)
Rectangle	1	6e-5	7.143e-5	1.92e-4
	2	8e-5	7.143e-5	1.958e-4
	3	10e-5	7.143e-5	2e-4
Square	1	6.315e-5	6.514e-5	1.75e-4
	2	8.42e-5	6.514e-5	1.78e-4
	3	10.53e-5	6.514e-5	1.792e-4
Semi-circle	1	6.67e-5	5.83e-5	1.555e-4
	2	9.167e-5	5.83e-5	1.583e-4
	3	11.67e-5	5.83e-5	1.61e-4
Triangle	1	7.5e-5	5.435e-5	1.52e-4
	2	10e-5	5.435e-5	1.532e-4
	3	13.33e-5	5.435e-5	1.553e-4

From Table 4.2 it can be observed that the value of the slopes remains constant in the ohmic region but the slopes change drastically in the activation region. The less the slope the better is the performance. Increasing the temperature decreases the activation loss and therefore decreasing the slope of the j-V curve at the activation region.

4.5 Pressure Variation

The operating pressures of the fuel cell are varied from 1 atm on both anode and cathode sides to 2 atm on the anode side and 4 atm on the cathode side, and the j-V curves are calculated to check the performance of the fuel cell. The operating pressure is again changed from 2 atm and 4 atm at the anode and cathode side to 3 atm and 5 atm at the cathode side. Figs 4.17, 4.19, 4.21 and 4.23 represent the j-V curves of the different channel geometries at different operating pressures. Figs 4.18, 4.20, 4.22 and 4.24 represent the power density curves of different channel geometries at different operating pressures.

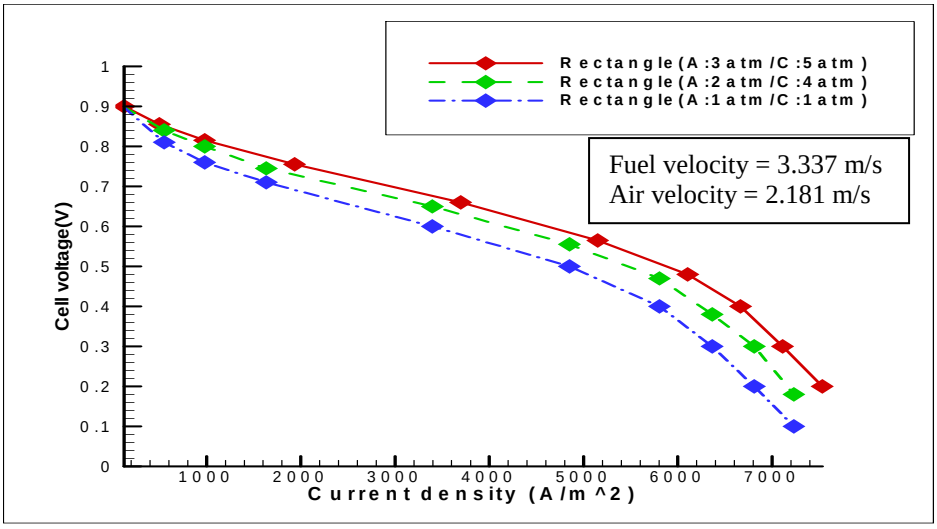

Fig 4.17 j-V curves of the rectangular channel at various operating pressures

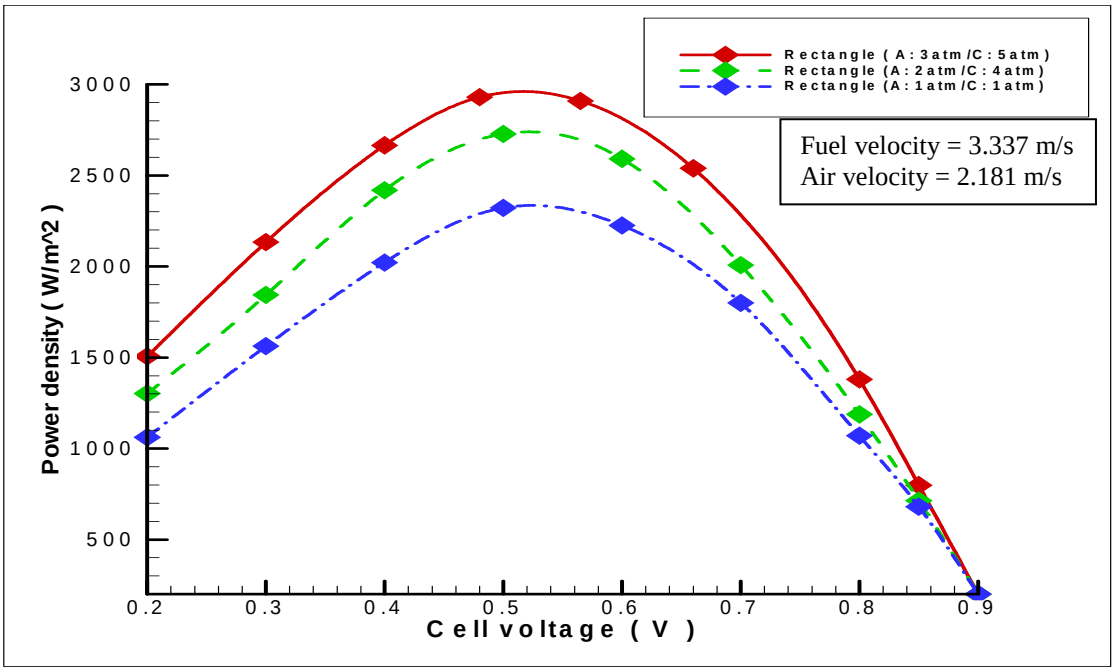

Fig 4.18 Power density curves of the rectangular channel at various operating pressures

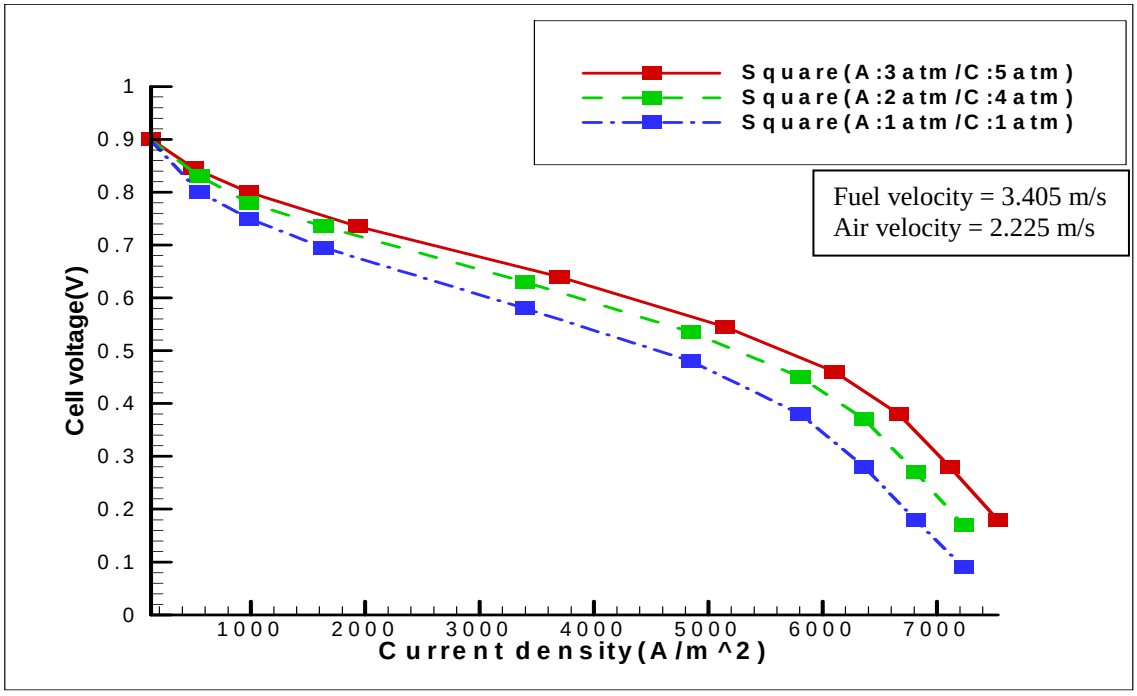

Fig 4.19 j-V curves of the square channel at various operating pressures

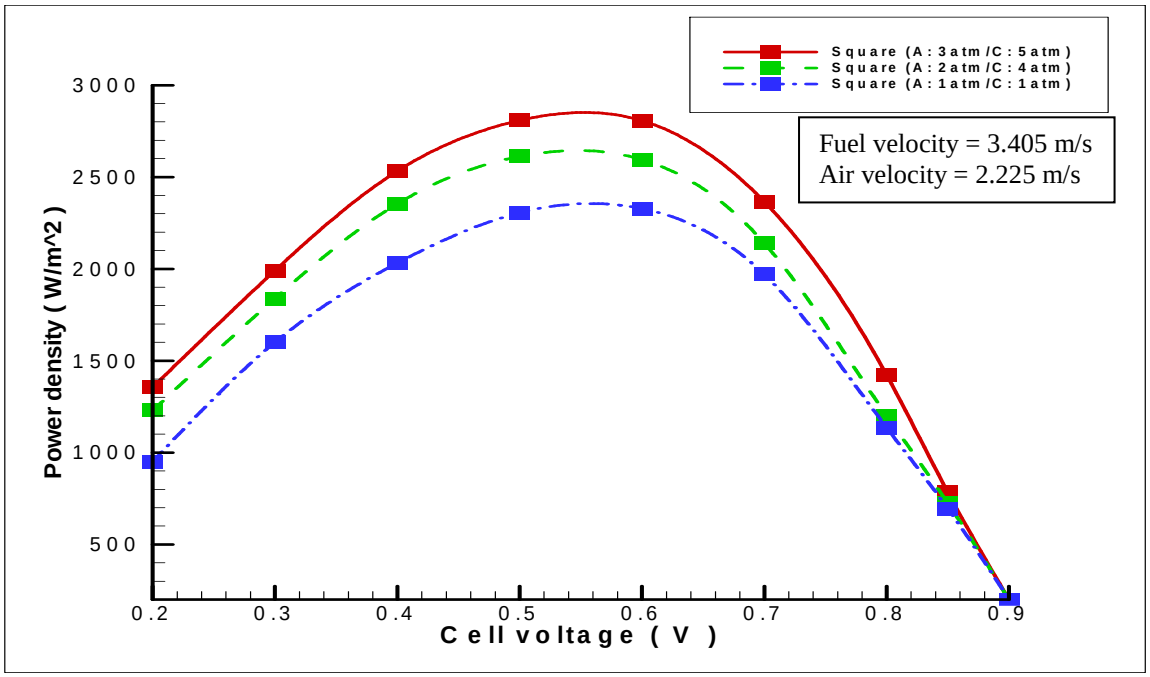

Fig 4.20 Power density curves of the square channel at various operating pressures

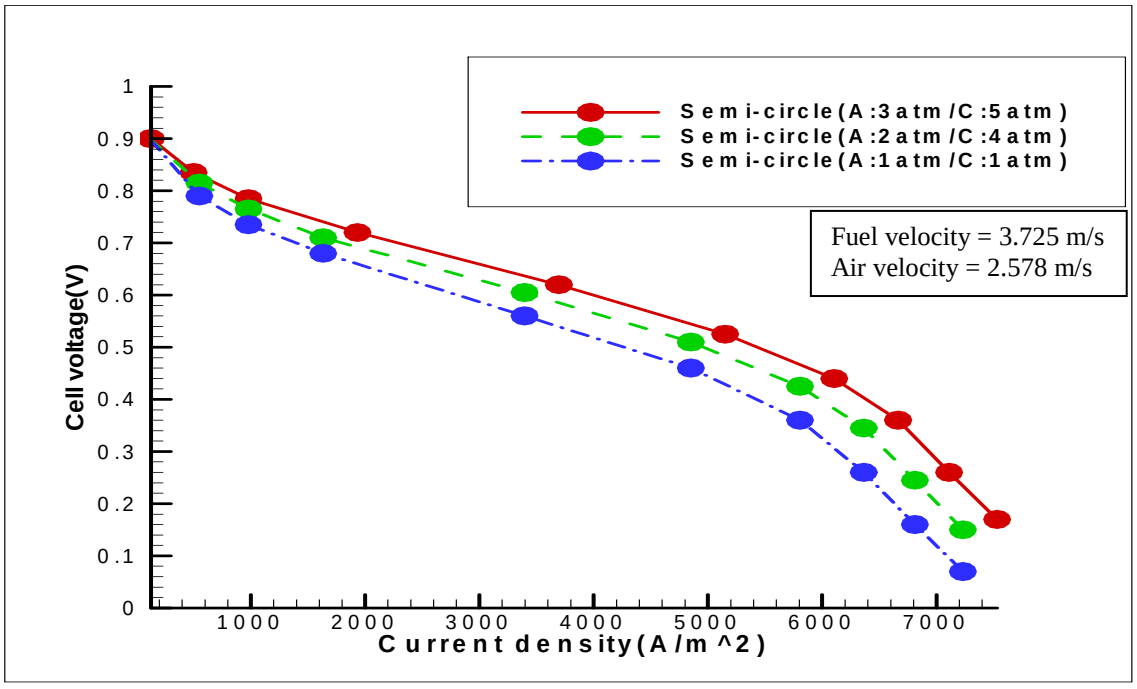

Fig 4.21 j-V curves of the semi-circular channel at various operating pressures

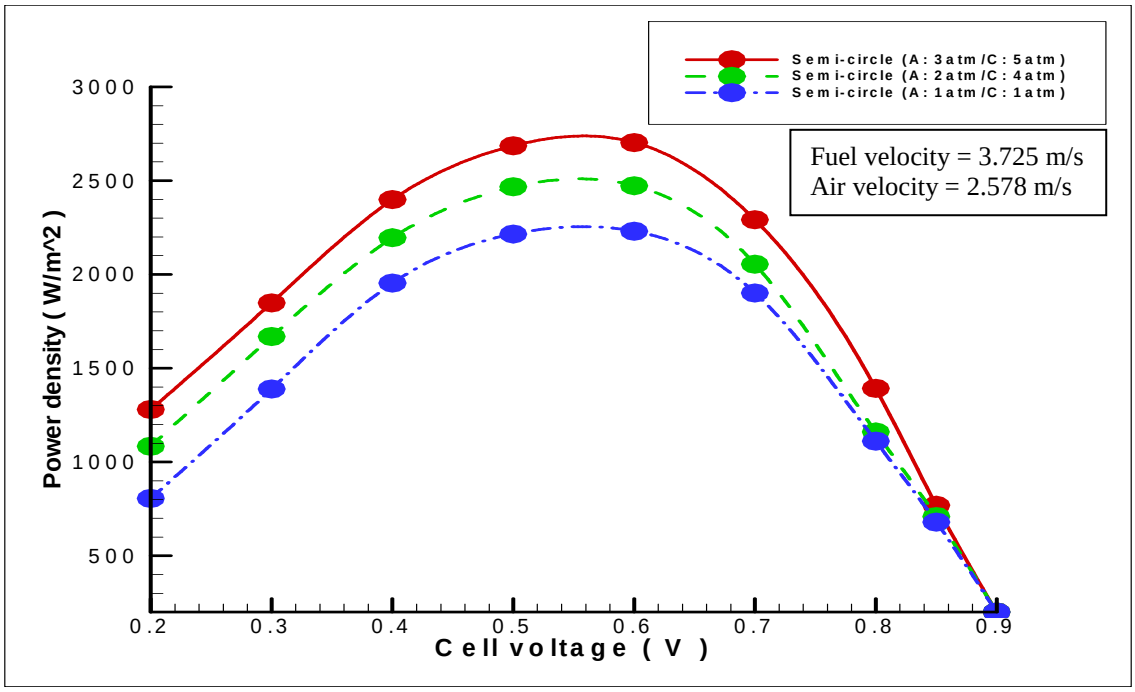

Fig 4.22 Power density curves of the semi-circular channel at various operating pressures

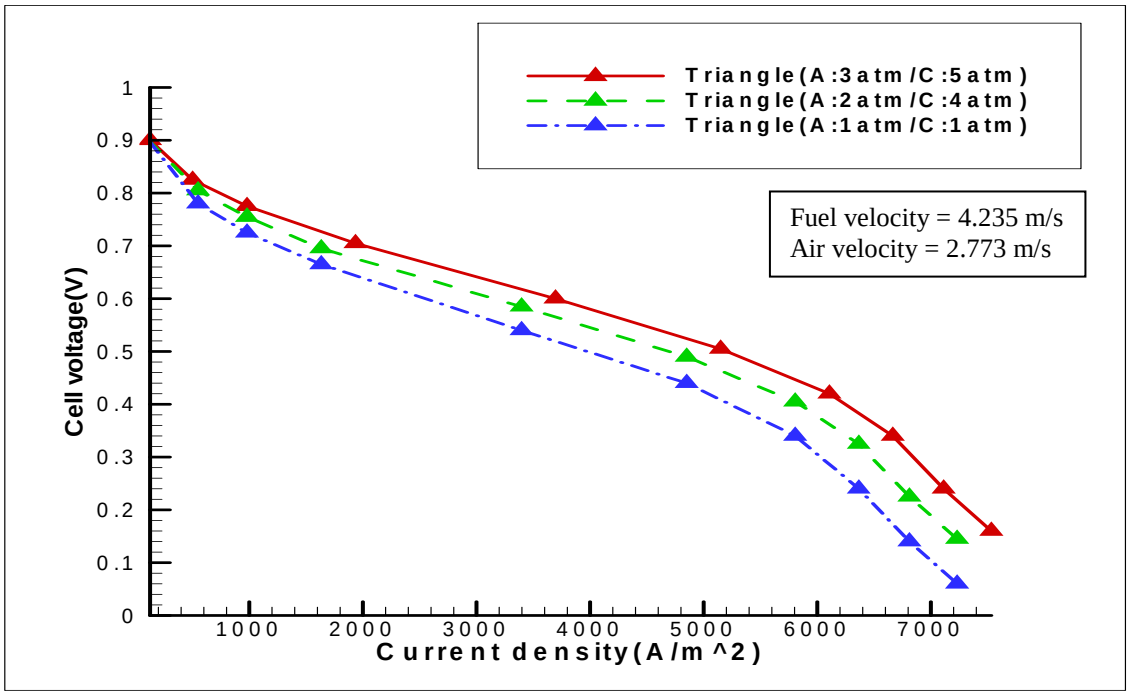

Fig 4.23 j-V curves of the triangular channel at various operating pressures

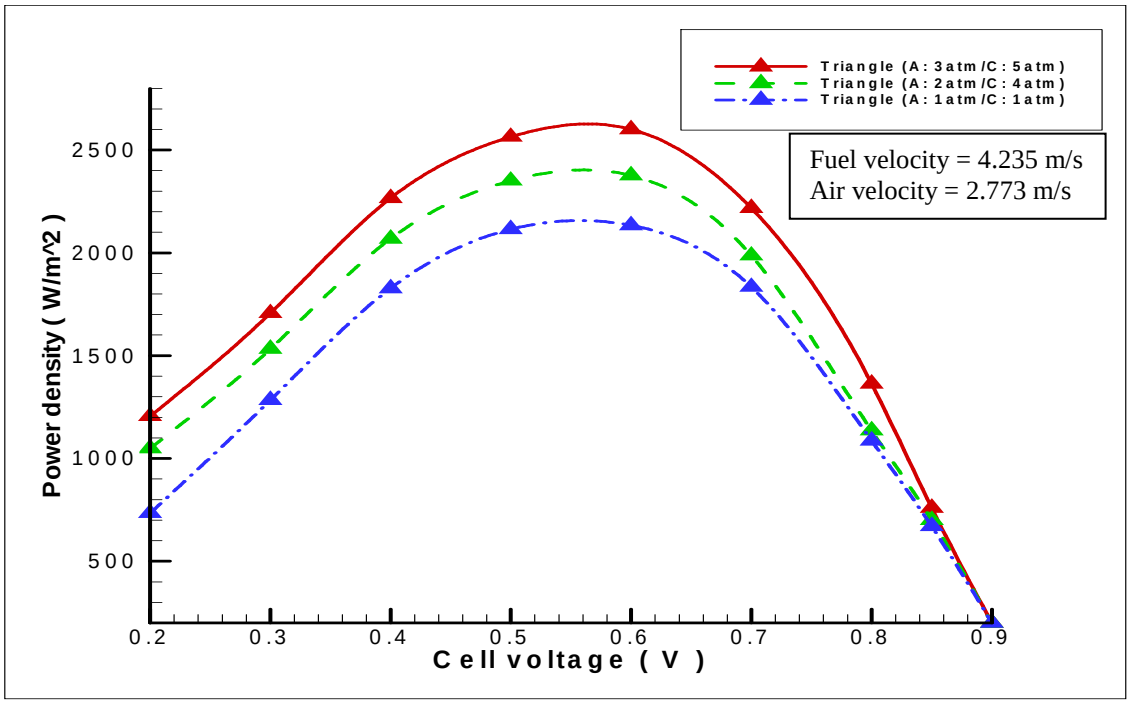

Fig 4.24 Power density curves of the triangular channel at various operating pressures

Increasing the pressure has less effect on the performance of the fuel cell when compared with increasing temperature. The solid line in Figs 4.17, 4.19, 4.21 and 4.23 represents the j-V curve of the fuel cell at an operating pressure of 3 atm on the anode side and 5 atm on the cathode side. The dashed line Figs 4.17, 4.19, 4.21 and 4.23 represents the j-V curve of the fuel cell at an operating pressure of 2 atm on the anode side and 4 atm on the cathode side. The dashed dot line in Figs 4.17, 4.19, 4.21 and 4.23 represents the j-V curve of the fuel cell at an operating pressure of 1 atm at both the anode and cathode side. From Figs 4.17, 4.19, 4.21 and 4.23 it can be observed that the performance increases with increasing the operating pressure. The slopes of the j-V curves are tabulated in Table 4.3.

Table 4.3 Slopes of the j-V curves at different operating pressures

Shape of the channel	Pressures (1.A: 3atm/C: 5atm), (2.A: 2atm/C: 4atm) and (3.A: 1atm/C: 1atm) Slope			
	Activation region (400 – 1000 A/m^2)		Ohmic region (2000 – 4200 A/m^2)	Concentration region (5500 – 6400 A/m^2)
Rectangle	1	8e-5	5.88e-5	1.23e-4
	2	8.25e-5	5.88e-5	1.535e-4
	3	8.45e-5	5.88e-5	1.78e-4
Square	1	9.375e-5	6.38e-5	1.18e-4
	2	9.436e-5	6.38e-5	1.35e-4
	3	9.532e-5	6.38e-5	1.462e-4
Semi-circle	1	10.05e-5	7.1e-5	1.15e-4
	2	10.22e-5	7.1e-5	1.362e-4
	3	10.35e-5	7.1e-5	1.523e-4
Triangle	1	11.23e-5	7.567e-5	1.083e-4
	2	11.375e-5	7.567e-5	1.253e-4
	3	11.489e-5	7.567e-5	1.476e-4

From Table 4.3 we can observe that slopes at the ohmic region remain the same and the slopes at the concentration region changes. The slope of the j-V curves decreases with increase in pressure. The less the slope the better is the performance. The concentration loss is decreased when the pressure is increased, so there is change in the

slope of the j-V curve at the concentration region. The performance of the fuel cell may be increased due to better supply of reactants at higher pressures to active sites near the front surface of the electrodes, which is the predominant reaction zone at higher current densities [8].

CHAPTER 5

CONCLUSIONS AND RECOMMENDATIONS

5.1 Conclusions

A single channel PEMFC is taken and validated by comparing the numerical results with the published experimental data in the literature. The obtained results are in good agreement with the available published experimental data. The validated parameters are then applied to the future designs. An improved design of the bipolar plate is developed for uniform flow. The flow channel geometry is changed to different shapes and the performance is observed. The conclusions pertaining to this research work are summarized as follows:

- Uniform flow distribution is obtained in the improved design of the bipolar plate. The baseline design has non-uniform flow distribution, the velocity high at the lateral channels and low at the center channels.
- The geometry of the channel is changed from the rectangular shape to square, semi-circle and triangular shapes and the performance of the fuel cell is observed. The rectangular channel has better performance when compared with the other channels. The reason for this may be due to the area that is in contact with the fluid flow. The triangular channel has the worst performance when compared with other channels.
- The operating temperature of the fuel cell is varied and the performance is observed. The performance of the fuel cell increases with increase in temperature. This is because as the temperature is increased the exchange current density is increased therefore increasing the performance of the fuel cell. Increasing the

reaction temperature increases the thermal energy available in the system and all the molecules in the system move about and vibrate with increased intensity increasing the rate of the reaction.

- The operating pressure of the fuel cell is varied and the resulting performance is observed. The performance of the fuel cell increases with increase in operating pressure. The increase in performance is very little when the pressure is increased. The increase in performance may be because of a better supply of reactants at higher pressures.

5.2 Recommendations

The electrochemical analysis is carried out using the COMSOL® software and due to the limitation on extensive memory requirement of COMSOL® only a single channel is selected to simulate the behavior of the PEMFC. Fuel cell module in Fluent can be used for detailed study of the PEMFC with huge number of elements, so that more accurate results can be obtained. If the fuel cell module in Fluent® is available a single PEMFC or a stack can be numerically analyzed. The change in the flow channel geometry should be studied in more detail. The performance of the whole fuel cell may be different from the single channel analysis. No experimental work has been done on the current design of the geometries of the channels. The experimental results can be used to validate the numerical simulations performed. A real time experiment may be carried out to know the exact behavior of each and every component of the fuel cell. The start up and shut down processes involved in the PEMFC can be studied. The flow in the channel is not fully developed. This led to overestimation of the numerical results when compared to

analytical results. The flow in the channel is not fully developed because the length of the channel is less than the developing length of the flow. The length of the channel should be increased to a length greater than the developing length to obtain fully developed flow in the channel.

REFERENCES

1. www.fuelcells.org
2. Ryan. O'Hayre, Suk-Won Cha, Whitney Colella, Fritz B. Prinz "Fuel cell fundamentals (2009)", John Wiley & sons, Inc, ISBN 9780470258439, 2nd edition, 2009
3. http://inventors.about.com/od/fstartinventions/a/Fuel_Cells.htm
4. http://americanhistory.si.edu/fuelcells/
5. D.M. Bernardi, M.W. Verbrugge, "A mathematical model of the solid polymer-electrolyte fuel cell," Journal of Electrochemical Society 139 (9) (1992) 2477–2491.
6. S. Dutta, S. Shimpalee, J.W.Van Zee, "Three-dimensional numerical simulation of straight channel PEM fuel cells," Journal of Applied Electrochemistry. 30 (2000) 135–146
7. T. Berning, D.M. Lu, N. Djilali, "Three-dimensional computational analysis of transport phenomena in a PEM fuel cell," Journal of Power Sources 106 (2002) 284–294.
8. E.A. Ticianelli, C.R. Derouin, A. Redondo and S. Srinivasan, "Methods to Advance Technology of Proton Exchange Membrane Fuel Cells," J. Electrochm. Soc. 135 (9) (1988) 2209–2214.
9. P.C. Sui, S. Kumarb, N. Djilali "Advanced computational tools for PEM fuel cell design Part 1. Development and base case simulations," Journal of Power Sources 180 (2008) 410–422

10. P.C. Sui, S. Kumarb, N. Djilali “Advanced computational tools for PEM fuel cell design Part 2. Development and base case simulations,” Journal of Power Sources 180 (2008) 423–432
11. R.F. Mann, J.C. Amphlett, M.A.I. H.M. Hooper, Jensen, B.A. Peppley, P.R. Roberge, “Development and application of a generalized steady-state electrochemical model for a PEM fuel cell,” Journal of Power Sources, 86, pp. 173-180, 2000.
12. P.T. Nguyen, T. Berning, Djilali, “Computational model of a PEM fuel cell with serpentine gas flow channels,” Journal of Power Sources, 130, pp. 149-157, 2004
13. S.Dutta , Sirivatch Shimpalee , J.W. Van Zee ” Numerical prediction of mass-exchange between cathode and anode channels in a PEM fuel cell,” International Journal of Heat and Mass Transfer 44 (2001) 2029-2042.
14. A.Kazim, H.T. Liu and P. Forges “Modelling of performance of PEM fuel cells with conventional and interdigitated flow fields,” Journal of Applied Electrochemistry 29: 1409 -1416, 1999.
15. J. Park, X. Li, “An experimental and numerical investigation on the cross flow through gas diffusion layer in a PEM fuel cell with a serpentine flow channel,” Journal of Power Sources, 163, pp. 853- 863, 2007.
16. S.A. Grigoriev, A.A. Kalinnikov, V.N. Fateev, A.A. Wragg, “Numerical optimization of bipolar plates and gas diffusion layers for PEM fuel cells,” Journal of Applied Electrochemistry, 36, pp. 991-996, 2006.
17. J. Wind, R. Spah, W. Kaiser, G. Bohm “Metallic bipolar plates for PEM fuel cells,” Journal of Power Sources 105 (2002) 256–260.

18. E.A. Cho, U.S. Jeon, H.Y. Ha, S.A. Hong, I.H. Oh, “Characteristics of composite bipolar plates for polymer electrolyte membrane fuel cells,” Journal of Power Sources, 125, pp. 178-182, 2004.
19. E. Sgrecciaa,d, M.L. Di Vona, S. Licoccia, M. Sganappa, M. Casciola, J.F. Chailan, P. Knauth “Self-assembled nanocomposite organic–inorganic proton conducting sulfonated poly-ether-ether-ketone (SPEEK)-based membranes: Optimized mechanical, thermal and electrical properties,” Journal of Power Sources 192 (2009) 353–359.
20. Qiangu Yan , Hossein Toghiani , Junxiao Wu “Investigation of water transport through membrane in a PEM fuel cell by water balance experiments”, Journal of Power Sources 158 (2006) 316–325.
21. Beuscher U., Cleghorn S.J.C., Johnson W.B., “Challenges for PEM fuel cell membranes”, International Journal of Energy Research, 29 (12), 1103-1112, 2005
22. L. Cindrella , A.M. Kannan, J.F. Lin, K. Saminathan, Y. Ho, C.W. Lin, J. Wertz “Gas diffusion layer for proton exchange membrane fuel cells—A review,” Journal of Power Sources 194 (2009) 146–160.
23. Xiao-Dong Niu, Toshihisa Munekata , Shi-Aki Hyodo, Kazuhiko Suga “An investigation of water-gas transport processes in the gas-diffusion-layer of a PEM fuel cell by a multiphase multiple-relaxation-time lattice Boltzmann model,” Journal of Power Sources 172 (2007) 542–552.
24. Jay Benziger , James Nehlsen, David Blackwell, Tom Brennan, Johannah Itescu “Water flow in the gas diffusion layer of PEM fuel cells” Journal of Membrane Science 261 (2005) 98–106.

25. Shengsheng Zhang, Xiao-Zi Yuan, Jason Ng Cheng Hin, HaijiangWang, K.Andreas Friedrich, Mathias Schulze. “A review of platinum-based catalyst layer degradation in proton exchange membrane fuel cells” Journal of Power Sources 194 (2009) 588–600
26. Feng-Yuan Zhang, Suresh G. Advani, Ajay K. Prasad, Mary E. Boggs, Shawn P. Sullivan, Thomas P. Beebe Jr. “Quantitative characterization of catalyst layer degradation in PEM fuel cells by X-ray photoelectron spectroscopy,” Electrochimica Acta 54 (2009) 4025–4030.
27. Prodip K. Das, Xianguo Li , Zhong-Sheng Liu “A three-dimensional agglomerate model for the cathode catalyst layer of PEM fuel cells,” Journal of Power Sources 179 (2008) 186–199.
28. Nawaz Akhtar, Arshad Qureshi, Joachim Scholta, Christoph Hartnig, Matthias Messerschmidt, Werner Lehnert. “Investigation of water droplet kinetics and optimization of channel geometry for PEM fuel cell cathodes” International Journal of Hydrogen Energy 34 (2009) 3104-3111.
29. J.K. Kuo, C.K. Chen, “A novel Nylon-6-S316L fiber compound material for injection molded PEM fuel cell bipolar plates,” Journal of Power Sources, 162 (1), pp. 207-214, 2006.
30. Xiao-DongWang, Yuan-Yuan Duan,Wei-Mon Yan, Xiao-Feng Peng, “Effects of flow channel geometry on cell performance for PEM fuel cells with parallel and interdigitated flow fields,” Electrochimica Acta 53 (2008) 5334–5343
31. COMSOL MULTI-PHYSICS user guide

32. T.A. Zawodzinski, T.E. Springer, S. Gottesfeld, “Polymer electrolyte fuel cell model,” Journal of the Electrochemical Society, v 138, n 8, Aug, 1991, p 2334-2342.
33. R.B. Bird, W.E. Stewart, and E.N. Lightfoot, Transport Phenomena, 2nd Edition, John Wiley & Sons, Inc., 2002.
34. Xiu Qing Xing, KahWai Lum, Hee Joo Poh, Yan LingWu “Geometry optimization for proton-exchange membrane fuel cells with sequential quadratic programming method” , Journal of Power Sources 186 (2009) 10–21.
35. R.K shah and A.L London. Laminar flow forced convection in supplement 1 to Advances in Heat Transfer, T.F. Irvine and J.P. Harnett (Eds.). Academic, New York, 1978.

VITA

Graduate College
University of Nevada, Las Vegas

Jephanya Kasukurthi

Degrees:

Bachelor of technology, Mechanical Engineering, 2007
Acharya Nagarjuna University, India

Selected publications:

[1] Jephanya Kasukurthi, K.M.Veepuri, J.H.Nie, Y.T. Chen, "Numerical Modeling of Velocity and Temperature Distributions in a Bipolar Plate of PEM Electrolysis Cell with Greatly Improved Flow Uniformity" ASME International Mechanical Engineering Congress and Exposition (IMECE2009-10519), November 13-19, 2009, Lake Buena Vista, Florida, USA

Thesis Title: Optimization of Channel Geometry in a PEM Fuel Cell

Thesis Examination Committee:
Chairperson, Yitung Chen, Ph. D.
Committee Member, Robert Boehm, Ph. D.
Committee Member, Jianhu Nie, Ph. D.
Graduate College Representative, Yahia Bagzhouz, Ph. D.